The role of *Cerl2* in cardiomyocyte differentiation and cardiac regeneration

João Paulo von Gilsa Lopes

Tese para obtenção do grau de Doutor em Mecanismos de Doença e Medicina Regenerativa

Doutoramento em associação entre:
Universidade NOVA de Lisboa (Faculdade de Ciências Médicas | NOVA Medical School)
Universidade do Algarve (UAlg)

Setembro, 2022

The role of *Cerl2* in cardiomyocyte differentiation and heart regeneration

João Paulo von Gilsa Lopes

Orientadores: Prof. Doutor José A. Belo, Professor Associado com Agregação da Faculdade de Ciências Médicas | NOVA Medical School

Doutor José Manuel Inácio, Investigador da Faculdade de Ciências Médicas | NOVA Medical School

Tese para obtenção do grau de Doutor em Mecanismos de Doença e Medicina Regenerativa

Doutoramento em associação entre:

Universidade NOVA de Lisboa (Faculdade de Ciências Médicas | NOVA Medical School)

Universidade do Algarve (UAlg)

Setembro, 2022

À minha avó Josefa e ao meu pai Zé.

Acknowledgements

Gostaria de começar por agradecer aos meus supervisores, Prof. Doutor José Belo e Doutor José Inácio, não só pela oportunidade de desenvolver este trabalho, mas também por todo o acompanhamento ao longo destes últimos quatro anos. Este trabalho de investigação teve o apoio financeiro da Fundação para a Ciência e Tecnologia (PD/BD/136919/2018 e COVID/BD/152624/2022), no âmbito do Programa Doutoral em Mecanismos de Doença e Medicina Regenerativa (ProRegeM). Gostaria também de agradecer a todas as pessoas da Nova Medical School e NMS Research com quem tive o gosto de trabalhar ou de me cruzar.

Quando há quatro anos embarquei nesta aventura, houve um grupo de pessoas que o fez comigo, e sem a presença dos quais teria sido consideravelmente mais complicado chegar até aqui, e aos quais agradeço a companhia. Em especial, gostaria de agradecer à Catarina Carvalho e ao Jorge Pontes pela amizade, pela confiança, e pelo conforto que sinto convosco. Agradecer também ao Oriol, à Graça, e à Matilde, que estiveram por perto desde o momento inicial, e assim se mantiveram.

O caminho de um doutoramento é por muitas vezes bastante solitário. Eu considero-me sortudo por raras vezes me ter sentido assim, independentemente da distância física. Obrigado aos que se mantiveram por perto, Jorge, Catarina, Pedro, e Ana Lurdes. Obrigado às que chegaram entretanto, Sabrina e Mafalda. Agradecer também à família que escolhi e me escolheu, rodeando-me desde que cheguei a Lisboa

há 10 anos, obrigado Ana Filipa, Nuno, e Zé Pedro. E obrigado a toda família que deixei no Alentejo, e que não raras vezes se queixou da minha distância. Em especial, obrigado São e mano Guilherme, com os quais tive de enfrentar situações bem mais complicadas que uma experiência falhada.

À minha irmã Teresa gostava de agradecer o exemplo, a força, e o afeto que me deu todos estes 1663 dias de doutoramento. Não houve um único desses dias em que não te sentisse como a minha rede de segurança para o caso de tudo correr mal, e em vários desses dias pareceu que as coisas iam correr muito mal. Não sei se algum dia conseguirei agradecer o suficiente ou retribuir.

Por fim, e ainda que não haja palavras certas ou suficientes, obrigado Miguel.

Abstract

Cerberus-like 2, currently designated *DAN domain BMP antagonist family member 5* (*Dand5*), is a secreted molecule that serves as antagonist to Nodal/TGF-β and Wnt pathways. During development, this molecule has been reported as being crucial in establishing left-right (LR) body asymmetry. In a knockout (KO) mouse model, the depletion of this molecule lead to randomization of the LR asymmetry. Moreover, myocardial hyperplasia was also observed, independently of randomization defects. Prolonged Nodal/TGF- β signalling was indicated to be behind the thickening of myocardial walls, due to an increase in the mitotic index during embryonic development.

These results point out that DAND5 can also modulate cardiogenesis. As such, from the KO mouse model, mouse embryonic stem cells (mESCs) were derived and, using the embryoid body (EB) differentiation approach, used to study DAND5's possible role in cardiomyocyte differentiation. EBs allow spontaneous differentiation of mESCs, and resembles early embryonic development, serving as a window to the molecular and cellular processes of that period. *Dand5* KO EBs recapitulate the *in vivo* results, with cardiac features emerging first than in wild type (WT) EBs. Spontaneous contractile clusters, termed beating foci, appear in WT EBs around days 7-8 of differentiation, while in KO EBs these features

appear earlier, at days 6-7. Furthermore, KO EBs also display earlier expression of mesoderm and cardiac genes, such as *Brachyury* and *Nkx2.5*; more α-actinin staining with better sarcomere organisation; and higher number of cardiac progenitors. All in all, depletion of DAND5 during EB differentiation enhances cardiac differentiation, by inducing mesoderm and activating cardiogenic genes earlier.

In the work developed for this thesis, these results were further substantiated by a subsequent RNA sequencing (RNAseq) dataset comprising data from both WT and KO EBs at various timepoints of the differentiation, that showed the same genetic expression trend. For example, genes encoding cardiac cells calcium channels (*e.g., Cacnb2*) or sarcomeric proteins (e.g., *Tnnt2* or *Myh6*), were expressed earlier in KO EBs. The RNAseq data provided a widened view into the changes resulting from DAND5's absence, showing that, overall, KO EBs progress faster through differentiation. The differences in expression will lead to differences in expression of genes involved with Notch and Wnt signalling pathways, as well as changes in expression of genes encoding membrane proteins (*e.g.*, *Itb3*, an integrin subunit). These distinct expression profiles will fundamentally alter cellular signalling and how cells interact with their microenvironment.

Wnt and Notch pathways have been involved in inducing and controlling epithelial to mesenchymal transition (EMT), a cellular process that transforms

tightly packed cells, changing their cytoskeleton, cell-cell, and cell-extracellular matrix (ECM) contacts, and genetic expression, culminating in acquisition of migratory potential. Bearing this in mind, and the RNAseq results showing disruption of EMT-related pathways, WT and KO EBs were studied regarding migration, genetic expression of EMT transcription factors (TFs) and membrane proteins, and presence of focal adhesions (FAs). Phenotypically, KO EBs show lower migration rates, with higher FA contents, denoting a stronger attachment to the substrate. As for EMT TFs and membrane proteins expression, the absence of DAND5 anticipates their expression.

One of the hallmarks of *in vivo* EMT processes is heart valve development, specifically termed endothelial to mesenchymal transition (EndMT). After an upregulation of ECM production at prospective valve sites, cells of the lining endocardium are patterned by Notch and BMP signalling pathways to enter EndMT. These cells, upon completing EndMT, will migrate into the ECM cushions, proliferate, and organize themselves into different layers, accordingly to the mechanical requisites of heart valves. The four heart valves will prevent retrograde flow within the heart, ensuring proper blood pumping. Given the *in vitro* results and the *in vivo* importance of EndMT, *Dand5* KO mice were screened for valve defects that could be correlated with the *in vitro* alterations in EMT. *Dand5* expression during valve development locates to the myocardium, also the source

of patterning BMP signal, and KO mice harbour valve morphological defects, namely inversion of the leaflets, which can compromise their function.

This thesis provides evidence that DAND5 range of action goes beyond early development. Its absence leads to significantly different expression patterns *in vitro*, as well as defects in EMT and migration. In line with these results, *in vivo* depletion of DAND5 influences heart valve development, causing leaflet inversion. Understanding the influence of DAND5 in EMT and cell transformation allows further understanding of its role in development, or even in some disease contexts, such as congenital heart defects.

Resumo

Cerberus-like 2, atualmente denominado *DAN domain BMP antagonist family member 5* (*Dand5*), é uma proteína extracelular cuja função é antagonizar várias vias de sinalização celular, como Nodal/TGF-β e Wnt. Estudos prévios associaram esta proteína ao correto estabelecimento da assimetria esquerda-direita na organização dos órgãos do tronco durante o desenvolvimento embrionário. Num modelo de ratinho em que o gene *Dand5* foi substituído, levando à sua ausência (*Dand5* KO, do inglês *knockout*), observou-se uma aleatorização da organização de órgãos como o coração, os pulmões, ou o estômago. Para além desses defeitos, e independentemente dos mesmos, ratinhos *Dand5* KO apresentavam hiperplasia do miocárdio, resultante do prolongamento da via de sinalização Nodal/TGF-β, que por sua vez causa um aumento do índice mitótico das células cardíacas durante o desenvolvimento embrionário. Estes resultados indicaram que o papel de *Dand5* podia ir além da correta organização do plano corporal, e foram o ponto de partida para uma estratégia *in vitro* que permitisse compreendê-los melhor. Obtiveram-se células estaminais pluripotentes com e sem o gene *Dand5*, *wild type* (WT) e KO, respetivamente. Recorrendo a estas células, desenhou-se uma experiência de diferenciação de corpos embrióides (*embryoid bodies*, EBs, em inglês), que

permite obter espontaneamente todos os tipos de células do organismo. Esta estratégia de diferenciação de células pluripotentes recapitula alguns eventos moleculares e celulares do desenvolvimento embrionário. Os EBs KO reproduziram *in vitro* os resultados obtidos *in vivo*, demonstrando uma diferenciação cardíaca antecipada. A presença de zonas espontaneamente contrácteis em EBs WT é notória por volta dos dias 7-8 do processo de diferenciação, enquanto em EBs KO estas zonas surgem mais cedo, por volta dos dias 67. Para além destas características fenotípicas, os EBs KO também expressam mais cedo genes associados com a mesoderme e o desenvolvimento cardíaco, como *Brachyury* ou *Nkx2.5*; produzem maiores quantidades de α-actinina, com uma organização melhorada; e dão origem a um maior número de progenitores cardíacos.

No trabalho desenvolvido para esta tese, estes resultados foram complementados com uma experiência de sequenciação de RNA (RNAseq), que incluiu amostras de ambos tipos de EB a diferentes alturas do processo de diferenciação. Estes resultados de expressão genética recapitularam a antecipação de expressão de genes envolvidos na cardiogénese. Entre os genes expressos antecipadamente encontravam-se genes codificando canais de cálcio cardíacos (*e.g.*, *Cacnb2*), proteínas sarcoméricas (*e.g.*, *Tnnt2* ou *Myh6*).

Os resultados da análise RNAseq permitiram alargar a análise dos efeitos decorrentes da ausência de DAND5 durante a diferenciação de EBs, mostrando

que os EBs KO diferenciam mais rápido que os WT. Mais especificamente, os distintos perfis de expressão conduzem a diferente expressão de genes envolvidos nas vias Notch e Wnt, tal como genes que codificam proteínas membranares (*e.g.*, *Itgb3*, uma subunidade de integrina). As diferenças em termos de expressão vão alterar fundamentalmente as vias de sinalização e a maneira como as células interagem com a sua envolvência.

As vias de sinalização Wnt e Notch foram reportadas como induzindo e controlando a transição epitélio para mesenquima (EMT, do inglês *epitelial to mesenchymal transition*), um processo celular que permite que células epiteliais, organizadas estaticamente em camadas compactas, sofram alterações do citoesqueleto, dos seus pontos de contacto com outras células e com a matriz extracelular (ECM, do inglês *extracelular matrix*), e da sua expressão genética. Todas estas alterações irão alterar o fenótipo das células e permitir que estas migrem. Tendo isto em consideração, e os resultados da análise RNAseq que demonstram alterações nas vias Notch e Wnt, estudaram-se defeitos de migração, expressão genética de genes relacionados com a EMT, e a presença de adesões focais em EBs WT e KO. Fenotipicamente, EBs KO migram menos, e têm mais adesões focais, denotando uma maior adesão ao substrato. Já a expressão genética de genes encarregues de induzir e controlar a EMT, observou-se uma antecipação da sua expressão em EBs KO.

Um dos processos de EMT mais característicos *in vivo* é o desenvolvimento das válvulas cardíacas, especificamente chamado transição endotélio para mesenquima (EndMT, do inglês *endotelial to mesenchymal transition*). Durante este processo, e após um pico de produção de ECM nos locais das futuras válvulas, a ativação das vias Notch e BMP desde o miocárdio vai levar a que as células do endocárdio entrem na EndMT. Após adquirirem capacidades migratórias, estas células vão infiltrar as acumulações de ECM, onde vão proliferar e organizar-se de modo a exercerem a sua função e de acordo com as especificidades mecânicas do coração. As quatro válvulas cardíacas vão impedir a regurgitação de sangue entre as diferentes partes do circuito cardiovascular. Dados os resultados *in vitro*, e a importância fisiológica da EndMT, os ratinhos KO foram analisados, de modo a perceber se as alterações *in vitro* ao nível da EMT tinham alguma tradução para o contexto animal. A expressão de *Dand5* na altura do desenvolvimento valvular localiza-se no miocárdio, o local responsável por ativar a via BMP. Para além disso, os ratinhos KO apresentam defeitos morfológicos nas válvulas cardíacas em desenvolvimento, nomeadamente, uma inversão da organização dos folhetos valvulares, que pode eventualmente comprometer a sua função.

O trabalho desenvolvido nesta tese demonstra que o papel de DAND5 vai muito além do início do desenvolvimento. A sua ausência provoca padrões de expressão genética significativamente diferentes e defeitos na EMT e na

migração *in vitro*. No seguimento destes resultados, a ausência de DAND5 vai influenciar o desenvolvimento de válvulas cardíacas *in vivo*, provocando inversão dos folhetos valvulares. Estudar a influência de DAND5 em EMT e transformações celulares permite perceber melhor como é que esta molécula influencia não só o desenvolvimento, mas também contextos patológicos, tais como defeitos cardíacos congénitos.

Table of Contents

List of Figures

List of Tables

List of Abbreviatures

A
AJ – Adherens junction
AV – Atrioventricular
AVC – Atrioventricular canal
AVE – Anterior visceral endoderm

B
BMP – Bone morphogenetic protein
BSA – Bovine serum albumin

C
Cdh1 – Cadherin 1/E-Cadherin
Cdh2 – Cadherin 2/N-Cadherin
CM – Cardiomyocyte
CPM – Counts per million reads mapped

D
DAND5 – DAN domain BMP antagonist family member 5
DEG – Differentially expressed gene
DPBS – Dulbelcco's phosphate-buffered saline
DVE – Dorsal visceral endoderm

E
E – Embryonic day
E/M – Epithelial-mesenchymal
EB – Embryoid body
EC – Endothelial cell
EMT – Epithelial to mesenchymal transition
EndMT – Endothelial to mesenchymal transition

F
FA – Focal adhesion
FDR – False discovery rate
FHF – First heart field

H
HA – Hyaluronan
HT – Heart tube

I
IFT – Inflow tract

K
KO – Knockout

L
L-R – Left-right
LA – Left atrium
LV – Left ventricle

M
mESC – Mouse embryonic stem cells

MET – Mesenchymal to epithelial transition
ML – Midline

O
O/N – Overnight
OFT – Outflow tract
ORA – Over-representation analysis

P
PA – Pulmonary artery
PCA – Principal component analysis
PFA – Parafolmaldehyde
PHT – Primitive heart tube
PS – Primitive streak

R
RA – Right atrium
RNAseq – RNA sequencing
RT – Room temperature
RT-qPCR – Real time quantitative polymerase chain reaction
RV – Right ventricle

S
SHF – Second heart field
SL – Semilunar
SMC – Smooth muscle cell

T
TF – Transcription factor
TGF-β – Transforming growth factor β
TJ – Tight junction
TPM – Transcripts per million

V
VEC – Valve endothelial cell
VIC – Valve interstitial cell

W
WT – Wild type

Z
ZEB – *Zinc finger E-box binding*

Chapter 1 - General Introduction

1.1 Mouse Heart Development

Among the many animal models, the mouse is the one that closely resembles humans, and robust correlations between embryonic events of these two different species can be established. In spite of morphological differences, mouse heart development is quite similar to human cardiogenesis[1]. Mouse heart development has been the focus of developmental biologists for some time, and its development, as well as its function, are far from being completely understood.

1.1.1 Morphological cardiogenesis

After being one of the structures to spearhead embryonic development, the mouse embryo heart is fully formed at around Embryonic day (E) 14.5[2]. The heart's developmental journey starts at the pre-streak stage, around E6.0, when the mouse embryo comprises the extraembryonic ectoderm, a pluripotent cell population (epiblast), and a layer of visceral endoderm. Following a series of signalling events, the embryo will be patterned to develop an anterior-posterior axis[3]. At the posterior side of the embryo, an important developmental structure will emerge, the Primitive Streak (PS), while the anterior side of the embryo is termed Midline (ML). The next step in mouse embryonic development,

gastrulation, is dependent on PS formation[4]. During this morphological and molecular event, undifferentiated cells of the epiblast migrate through the PS[5], and are subjected to molecular signals that will determine their cellular fate[6] (Figure 1.1). At the end of gastrulation, epiblast cells will have transformed, migrated through the PS, and further differentiated, giving origin to the three germ layers of the embryo: ectoderm, mesoderm, and endoderm[7]. The first cells to ingress will give origin to mesoderm, the next cells to the future endoderm, and, lastly, cells that will differentiate into the future ectoderm[8]. This ingression order will make it so that gastrulation inverts the spatial arrangement of germ layers on the epiblast[8].

The first cells to ingress through the PS will bilaterally migrate towards the anterior part of the embryo[5]. Once these two cell populations arrive to their ML destination, they will fuse[9] and start organising themselves into a horse-shaped structure, customarily called cardiac crescent (Figure 1.1), that can be subdivided in two distinct cell populations[10,11]: First Heart Field (FHF) and Second Heart Field (SHF). FHF cells will enter cardiac differentiation first, giving origin to the Primitive Heart Tube (PHT)[10], mainly composed of cells patterned to become Cardiomyocytes (CMs). The FHF cells will largely follow the cardiomyogenic program and give rise to all the myocardium of the Left Ventricle (LV) of the heart, and contribute partially to the myocardial walls of the Right Ventricle (RV) and of the Atria[10]. Cells from the SHF reside posterior to the PHT, where they will be kept

undifferentiated and proliferative[11] (Figure 1.1). SHF cells are progressively added to the cranial pole of the PHT, giving origin to the Outflow Tract (OFT) of the PHT[12]. These cells can differentiate into a wider range of cell types[13], from CMs to Endothelial Cells (ECs), or even Smooth Muscle Cells (SMCs).

As cardiogenesis progresses, the extending PHT will give place to the Heart Tube (HT), and in time it will start looping to the right side[2] (Figure 1.1). At the same time, further extension of the OFT at the arterial pole with SHF-derived cells, will give rise to what will be the RV[10]. At the venous pole of the HT, a similar mechanism will form the Inflow Tract (IFT) of the heart, the foundation for atria. Concomitantly with further growth and looping, the developing heart will experience organised cell differentiation events, that will lead to the maturation of the myocardial wall, and to the emergence of trabeculae, coronary vasculature, valve, and septa. Extension of the IFT, and further anterior looping that will bring the IFT upward of the HT, will allow the formation of the atria (Figure 1.1), Later stages of development will septate the OFT into the Pulmonary artery and the Aorta and the HT into two ventricles.

Apart from the heart fields, there are two additional cell sources that will contribute to cardiogenesis. A third cell population originates from the Proepicardial Organ, a transient structure located at the caudal end of the developing heart, that will contribute towards the formation of the epicardium, an outer layer of cells[13]. The neural tube constitutes the fourth cell source for

cardiogenesis[12]. The cells that delaminate from that region and cooperate in cardiogenesis are called Cardiac Neural Crest Cells. They will play an important role in the differentiation of the heart's conduction system, contribute to heart valves, and have a role in OFT patterning and septation as well[14].

Functionally, the heart is responsible for securing blood flow, blood oxygenation, nutrient delivery, and metabolite clearance. Deoxygenated blood will enter the heart through the Venae Cavae into the Right Atrium (RA). It will then be pumped into the RV and exit the heart through the Pulmonary Artery (PA), heading towards the lungs. Upon return, oxygenated blood enters the heart via Pulmonary Veins, into the Left Atrium (LA). It then passes to the LV, before departing the heart through the Aorta, in direction to the organs. Unidirectional blood flow and pumping is further secured by cardiac valves. Two of these structures are located between atria and ventricles, the atrioventricular valves, and the other two between ventricles and the arteries, the semilunar valves.

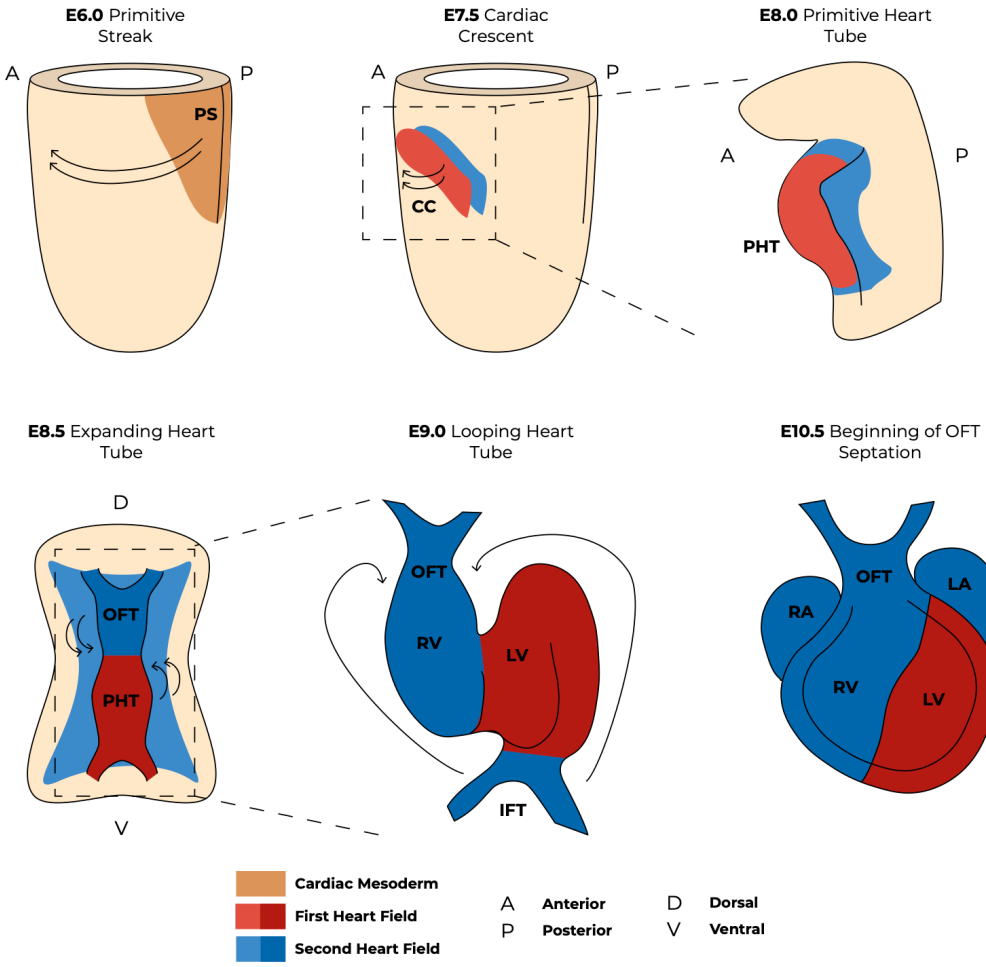

Figure 1.1 - Schematic of mouse heart development. (PS – Primitive Streak; CC – Cardiac Crescent; PHT – Primitive Heart Tube; OFT – Outflow Tract; HT – Heart Tube; RV – Right Ventricle; LV – Left Ventricle; IFT – Inflow Tract; RA – Right Atria; LA – Left Atria)

Cardiac function is secured by a cardiac wall organisation that encompasses three different layers: epicardium, myocardium, and endocardium. The epicardium serves not only as a covering layer, but also as source of cells and a signalling hub to the myocardium[15,16]. Moreover, epicardium cells provide signalling cues during development for correct establishment of coronary

vasculature. The myocardium is the middle layer of the heart wall and is *de facto* responsible for blood pumping. This contractile layer is mainly composed by a contractile syncytium formed by CMs, while containing cardiac fibroblasts, cells of the cardiac conduction system, and capillaries to ensure correct blood supply[2]. The endocardium can be found covering the luminal side of the heart wall and is composed of endothelial cells[17,18]. The main function of this inner layer is to separate blood flow from the myocardium and its vasculature.

During cardiac development, the inner side of the myocardium will develop finger-like muscle projections called embryonic trabeculae. The emergence of these structures is necessary for efficient cardiac pumping in the developing embryo, as well as for the development of the cardiac conduction system[19]. Trabeculae are responsible for mechanically increasing contraction while promoting CM proliferation and providing blood supply to the embryonic cardiac wall. The next step in heart development has been termed compaction, being defined as a “collapse” of the trabeculae into compact myocardium. The myocardium of a mature heart is mostly composed of a compact layer of CMs[2]. Regarding the cellular events behind maturation of the myocardial wall structure, a specific inactivation of *Notch2* has been described as being necessary for proper myocardial structural and functional development[20].

1.1.2 Cell signalling events during cardiac development

Gastrulation induction with subsequent mesoderm emergence is dependent on epiblast cells undergoing Epithelial to Mesenchymal Transition (EMT)[4,21], a molecular process that changes cells and allows them to migrate away from their original location. Through Nodal expression at the proximal epiblast[22] and expression of Wnt inhibitors from the Anterior Visceral Endoderm and Distal Visceral Endoderm regions[23], at the pre-gastrulation stage (around E6.0), the embryo signalling dynamics will promote EMT and PS formation at the posterior side[4]. Simultaneously, the posterior epiblast will express WNT3A, a canonical Wnt pathway ligand that has been shown to also induce *Brachyury* expression[24], the first molecular hallmark of mesoderm specification. Together, they will be responsible for the induction of the PS[25]. At the same time, *Brachyury* will be responsible for inducing *Mesp1* expression in cells poised to form cardiac mesoderm[26]. This molecule is a transcription factor (TF) that plays a specific role within cardiogenesis, promoting EMT on the Posterior Epiblast, driving oriented cell migration, and upregulating cardiac genes[27].

Mesp1 is expressed in cells moving through the PS from E6.25 until E8.0. These cells can be divided into two different populations, according to *Mesp1* expression time window. Early *Mesp1* expression, from E6.25 until around E7.0, directs cells towards the FHF, while cells that pass through the PS and express *Mesp1* later, up to E8.0, will form the SHF[13]. This temporal division in expression

will limit cells' differentiation potential. The first subset of cells to express *Mesp1* will have the potential to become either CMs or ECs[13]. Some of these cells will also give origin to epicardium-derived cells progenitors. Late expression of *Mesp1* makes it so that cells of the SHF will display a wider differentiation potential, allowing them to differentiate into all cell types of the heart[13,28]. The patterning role of MESP1 is possible due to its numerous target genes, that include major cardiac transcription factors, such as *Mef2c*, *Tbx20*, *Gata4*, and *Nkx2-5*[29], as well as heart field-specific genes, *Hand2* for FHF[30], and *Foxh1* and *Tbx1* for SHF[31,32].

Besides *Mesp1* patterning, migratory cells of FHF will be exposed to canonical Wnt inhibiting molecules, driving them to start differentiating into cardiac lineage cells[33]. At the same time, these cells will be exposed to bone morphogenetic protein (BMP) and fibroblast growth factor (FGF) pathway activators, which will be important to sustain expression of cardiac TFs such as *Nkx2.5* or *Gata4*[33]. Upon reaching their ML, FHF cells will upregulate *Wnt11*[33], thereby activating non-canonical Wnt, a promotor of cardiac differentiation. As mentioned before, cells of the FHF will quickly give origin to the PHT, while SHF cells keep proliferating due to persistent activation of canonical Wnt pathway[34,35]. These cells are characterised by persistent *Isl1* expression, associated with proliferation maintenance[11]. As they progressively migrate towards the venous and arterial poles of the PHT, they will exit the proliferative state and, in similar fashion to FHF, inhibit canonical Wnt while activating BMP and FGF pathways,

thus entering cardiac differentiation[34,36]. Further differentiation into the different cell types of the heart requires a complex signalling network[15,36,37], in which all layers of the heart are involved in a specific way. A prime example of that is the role Notch signalling cues from ECs play in cardiomyocyte proliferation and differentiation[38]. Specific endocardial deletion of *Notch1* has been shown to lead to affect trabeculation by impairing CMs proliferation and ventricular differentiation[39]. Further studies in zebrafish have shown a signalling crosstalk between Notch and Wnt pathways that secures CM proliferation in the regenerating heart[40].

Heart looping starts even before the heart tube is completed, at around E9.0[41]. This process is thought to be closely related with chamber expansion and further OFT and IFT extension[42]. With the exception of the Atrioventricular (AV) region and the OFT, embryonic myocardium will express *Tbx20*, a TF that will induce and control the cardiogenic expression program[43]. This TF is able to interact with different gene regulatory networks[44]. In the SHF, TBX20 inhibits *Isl1* expression[45], promoting differentiation. In the future heart chambers, it elicits expression of chamber markers such as *Hey2* or *Mef2c*[44,45]. It also plays a role in expression of genes related to CM physiology, such as calcium and potassium channel genes[46]. Besides CMs, ECs and cardiac fibroblasts, there is another cell type important for heart physiology, the cells of the conduction system, responsible for coordinating cardiac contraction. These cells are differentiated

from cardiomyocytes of both FHF and SHF, in a location specific manner[47–49]. The signalling pathways involved in their differentiation have not been completely understood, but it is already clear that another Tbx gene, *Tbx3,* is responsible for downregulating cardiomyocyte chambers while upregulating pacemaker genes[50,51].

More advanced stages of heart development include septation and valve formation, and trabeculation/compaction. Due to its importance in this work, valve formation will be further explored in the next chapter.

1.2 Epithelial to Mesenchymal Transition

EMT is the process that leads epithelial cells to acquire a mesenchymal phenotype[52], as depicted in Figure 1.2. While epithelial cells are usually found within a tightly organised layer of other epithelial cells, mesenchymal cells can migrate and establish weaker and transient cell-cell and extracellular matrix (ECM) contacts. *In vivo*, cells can assume either one of these states, or even an intermediate epithelial-mesenchymal (E/M) state. This transformation, and its "opposite", Mesenchymal to Epithelial Transition (MET), are fundamental for proper embryonic development[4], tissue homeostasis[21], and even in some disease contexts, such as fibrosis or cancer[53]. Depending on the cellular context and outcome, EMT has been classified in three types[52]. In a developmental context, in which cells only acquire a non-aggressive migratory behaviour, EMT is classified as type I. A second EMT type occurs in wound healing situations and allows for tissue regeneration. If exacerbated, this type of EMT can lead to fibrosis, with subsequent loss of function. A type III EMT occurs in neoplastic cells, conferring them an invasive and aggressive phenotype, thereby contributing to cancer progression.

Type I EMT assumes a particularly important role during development. For example, PS formation and subsequent gastrulation require epiblast cells to undergo EMT[4,27], and proper organogenesis requires further MET and EMT. These embryonic transitions are characterized by a lack of invasive properties of

the resulting cells, and normally do not lead to fibrotic tissues. After embryonic development, EMT can assume both physiological and pathological roles. In an injury context, this transition is often required for proper wound healing, in association with inflammation[54,55]. This injury response can be exacerbated, resulting in fibrosis and pathological organ regeneration[56,57]. Another pathological context in which EMT plays a fundamental role is cancer progression[55]. Studies have demonstrated that EMT allows cancer cells to migrate away from their initial location, forming metastasis[58]. Additional reports have revealed that the implications of EMT in cancer progression extend beyond cancer cell escape[59,60]. It is becoming increasingly clear that EMT can confer advantageous features to cancer cells besides migratory potential, such as chemoresistance, immune evasion or metabolic rewiring[56].

Epithelial cells are usually found organised in tightly packed layers. These cells display strong apical-basal polarity, as well as a high number of cell-cell contacts[61]. These cellular interactions are mostly established through Adherens Junctions (AJs) and Tight Junctions (TJs)[61]. AJs bind directly to the actin cytoskeleton and intermediate filaments[62], while TJs ensure closed communication between cells. Mesenchymal cells are quite different, lacking apical-basal polarity and establishing weaker and less contacts with other cells. They are not tightly organised in a layer, but rather assume a morphology similar to a fibroblast, and use Focal Adhesions (FAs) to adhere to their

microenvironment[63]. Their migratory potential is often coupled with a pro-invasive behaviour, with secretion of ECM-degrading enzymes Matrix Metalloproteinase[64]. These two cell profiles are the prototypes of what is rather a phenotypical spectrum[65], resulting from the reversible nature of EMT and the fact that, at the end, cells can harbour features of both states[65,66].

Regardless of the context, the transcriptional and molecular players regulating EMT are similar and highly conserved[53]. Transcriptional regulation of EMT is mainly performed by three different TF families: *Snail*, *Twist*, and *zinc-finger E-box binding* (*ZEB*) factor[52]. From the three main EMT TFs, *Snail* displays a wider range of effects, including targeting the other EMT TFs (*e.g.*, ZEB TFs are a direct target of *Snail* TFs)[67,68].

E-Cadherin (*Cdh1*), which encodes the foremost epithelial AJ protein, will be the main target of the repressive effect of EMT TFs[52,69], while *N-Cadherin* (*Cdh2*) will be one of the most common targets for transcriptional activation[70]. Cytoskeleton intermediate filament proteins will also be targeted, with EMT TFs repressing the expression of *Cytokeratin*, while activating the expression of *Vimentin*[52,61]. This change will be coupled with a switch in membrane protein complexes and changes in cell-cell contacts. In epithelial cells, cytokeratin filaments bind to desmosomes and hemidesmosomes, responsible for cell-cell and cell-ECM adhesion, respectively[71]. Due to the stress resistance they confer, vimentin intermediate filaments allow mesenchymal cells to migrate[72]. These

filaments will bind to membrane integrins, that mediate mesenchymal cell adhesion to their surrounding ECM and cells. The changes in the cytoskeleton will also influence EMT, namely through their control on nucleus and organelles positioning[73], influencing another step in EMT: disruption of apical-basal polarity[74,75] and establishment of front-rear polarity in migrating cells.

There are several pathways that trigger EMT, and their influence is cell and organ specific[65]. Transforming growth factor beta (TGF-β) is often the responsible for activating EMT, by directly upregulating *Snail* and *ZEB*, as well as inducing *SMAD* expression[76]. The latter leads to an activation of canonical Wnt signalling, which will be further facilitated by the increasing cytoplasmatic concentration of β-catenin, from the disassembling AJs[77]. Interestingly, AJ breakdown can promote EMT on its own, through the release of β-catenin[78].

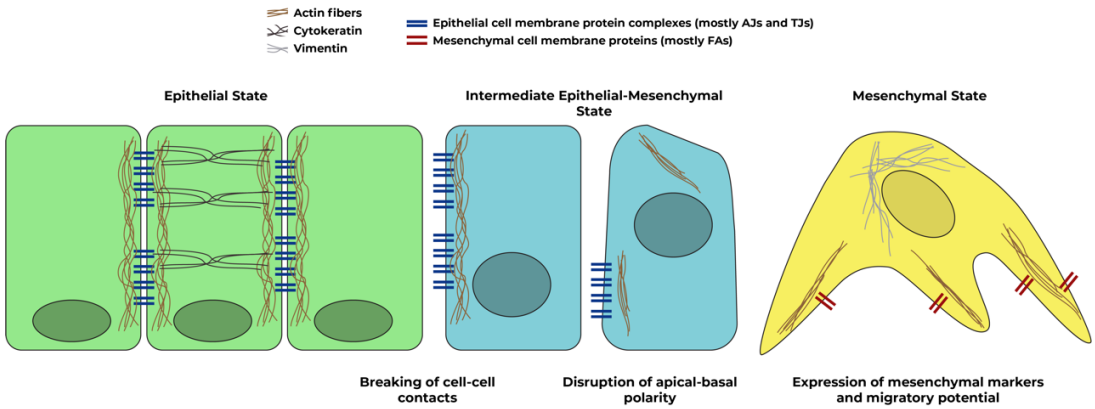

Figure 1.2 - Schematic representation of a typical EMT process. (EMT - Epithelial to Mesenchymal Transition)

Activation of EMT TFs initiates the process, with the consequent change in genetic expression and signalling activation. These changes will be followed by

remodelling of cell-cell and cell-ECM contacts, which will also alter membrane proteins (Figure 1.2). Simultaneously, this signalling network will alter the cell's cytoskeleton, influencing its polarity as well. These cellular events will culminate in the acquisition of migratory and invasive potentials. The range of possible EMT processes, combined with its multifactorial regulatory network, make it so that the cellular outcome is a spectrum between Epithelial and Mesenchymal cellular states[65].

1.2.1 Endothelial to Mesenchymal Transition in Heart Development

Within the range of cells and tissues that undergo EMT, there is a specific subtype of EMT during development that has been widely studied: Endothelial to Mesenchymal Transition (EndMT). This process, depicted on Figure 1.3, occurs in endothelial cells of the Atrioventricular Canal (AVC) and cells of the OFT, giving rise to cardiac valves. These structures ensure unidirectional blood flow and functional separation between the heart chambers[79]. Four valves can be found in the heart, two AV valves between atria and ventricles (mitral and tricuspid), and other two at the OFT, between the ventricles and the Pulmonary Artery and Aorta, the semilunar (SL) valves.

The developmental process of valve formation starts before any morphological changes can be seen, when myocardial cells at the AVC and OFT express *Bmp2* and *Bmp4*, which will restrict the location of the future heart

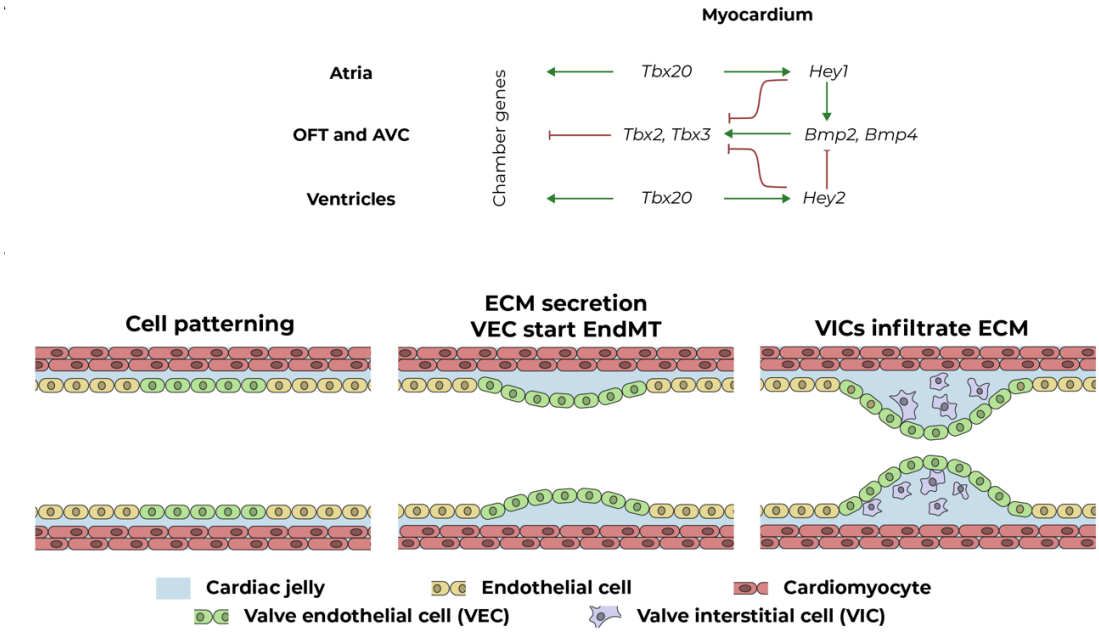

Figure 1.3 – A) Main genetic expression events behind valve patterning and EndMT (adapted from MacGrogan *et al.*); B) Schematic representation of EndMT process at cardiac valve sites. (ECM – Extracellular Matrix; EndMT – Endothelial to Mesenchymal Transition)

valves[80–82]. The expression of these two ligands will have two direct results at the AVC and OFT valve sites (Figure 1.3 A), the restriction of the expression of cardiac chamber markers[45] and induction of ECM production by myocardial cells[83]. A schematic for EndMT can be seen on Figure 1.3 B. The accumulation of ECM on AVC and OFT valve sites will lead to the emergence of endocardial cushions, the first morphological sign of valve differentiation. Initially, these cushions are just made of ECM, mostly Hyaluronan (HA), which has been found

to be necessary for correct valve development[83]. HA will activate the ErbB pathway axis, promoting expansion of the Valve Endothelial Cells (VECs) that line cushion sites[84]. At the same time, BMP from the myocardium and endocardial Notch activation will induce EndMT on a subset of VECs, by upregulating *Snail* TFs expression. The selected VECs will undergo EndMT, repressing endothelial contact points, migrating into the HA-rich cushions' matrix, and becoming Valve Interstitial Cells (VICs). After VICs migrate into endocardial cushions, the primitive valves display a simple and bulky structure. VEC proliferation will lead to valve elongation, while increased VIC number will allow further cellular occupation of the valve mesenchyme. These proliferative events are associated with BMP and Wnt signalling activation VICs and VECs, respectively.

Besides proliferation, VICs, VECs and valve ECM will undergo significant post-natal changes to transform endocardial cushions into mature valve leaflets. Transcriptomic analysis of post-natal valves has shown that the VEC population comprises different populations, depending on valve location and correlated with different levels of shear stress caused by blood flow[85]. In a similar way, valve mesenchyme will be organised according to the physical and mechanical properties[79,86,87]. Regarding ECM content, three different layers can be distinguished (Figure 1.4). The layer facing blood flow (termed Atrialis in AV valves and Ventricularis in SL valves) is mainly composed of elastin-rich ECM. In the middle of the valve mesenchyme, an ECM rich in proteoglycans can be found

(Spongiosa), while on the opposite side there is a predominance of collagen fibres (Fibrosa). VIC cell type changes drastically with valve maturation. Immature valves comprise cells that either express collagen, and are located at Fibrosa layer, or glycosaminoglycans, located mostly towards valve extremity. With maturation, four different cell populations will emerge[85], two of them responsible for ECM production and organisation, and two other responsible for immune system mediated processes.

The different heart valve types display significant morphological differences that can be seen on Figure 1.4, that ensure their function. AV valves include *Chordae tendinae*, fibrous projections that connect the fibrosa layer of the valve to the ventricular wall. During systole these structures prevent valvular collapse towards the atria, ensuring correct coaptation of AV valves. Cellular sources are also different, with Neural Crest Cells contributing towards the mesenchyme of SL valves, while also regulating septation of OFT into aorta and pulmonary artery.

Valvular function can be altered by stenosis or regurgitation, compromising valve function, and influencing overall cardiac physiology. Pathological valve function can be secondary to a cardiovascular pathology (*e.g.*, tricuspid regurgitation caused by right ventricle dilation). Primary valvular pathological situations can arise from developmental defects and/or dysfunctional ECM maintenance. The most common valvular defects resulting from developmental defects is Bicuspid Aortic Valve, where the aortic valve displays two leaflets

instead of three, and Mitral Valve Prolapse, when the mitral valve loses its physiological thickness, leading to valve insufficiency and retrograde blood flow. Alterations on ECM organisation or composition can also be detrimental. Through an increased content in proteoglycans that disrupts collagen and elastin fibres, valves will become thicker and unable to prevent regurgitation. In a similar fashion, pathological transformation of VICs associated with increased inflammation can disrupt normal Notch signalling and lead calcification of valves. This in turn leads to increased stiffness and stenosis[88].

Heart valve development is the result of a complex network of signalling pathways and mechanical cues. Throughout life, valvular function is dependent

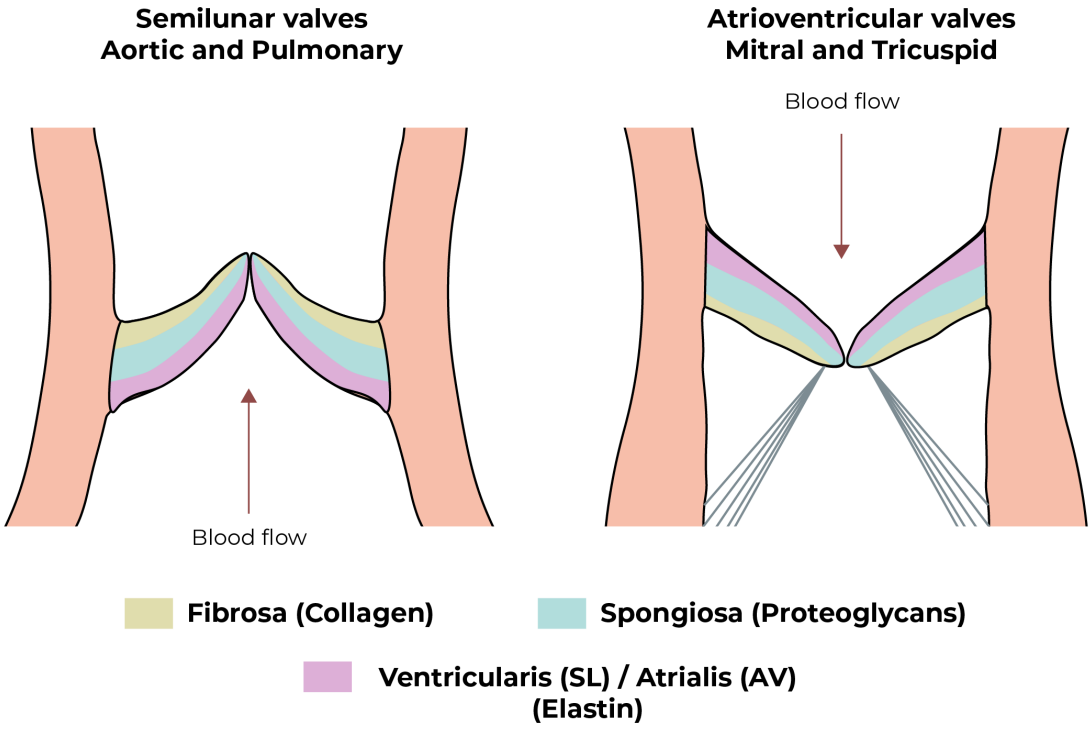

Figure 1.4 - Mature mouse heart valves morphological structure and ECM composition.

on the same pathways that guided embryonic development, that are also able to trigger pathological responses. Primary valve diseases result from either developmental defects of biomechanical changes that hinder their barrier role. Increased stiffness will lead to stenosis, while lower ECM resistance causes regurgitation. The effects of these pathologies in hemodynamics will end up compromising cardiac function.

1.3 Dand5

Originally called *Cerberus-like 2*, the DAN domain BMP antagonist family member 5 (DAND5[1]) gene is composed of two exons separated by a 5.92 kb intron, encoding a secreted glycoprotein[89]. This gene is part of the DAN gene family, which includes genes with a Cysteine-Rich Domain, that ensures their biological activity. These genes typically act as antagonists for the TGF-β pathway. In Mammals, this family comprises seven paralog genes: Neuroblastoma 1, Cerberus 1, Dand5, Sclerostin, Sclerostin domain containing 1, Gremlin 1, and Gremlin 2[90]. These genes have been reported as having a primary role during development, namely in the development of body axes and asymmetric body plan establishment.

In mice development, *Dand5* was initially reported as one of the first genes to break symmetric nodal expression, at around E7.5[89]. At such stages, *Dand5* expression is limited to the node, where post-transcriptional regulation induces mRNA degradation on the left side of the embryo[91]. Such regulation occurs on two different levels. The establishment of nodal fluid flow was shown to be the first regulatory step, through an influx of Ca^{2+} ions that will induce *Dand5* 3'-UTR

[1] Throughout this thesis, the most recent name will be preferred.

mRNA degradation. This will cancel the inhibition on WNT3, that, upon cytoplasmatic accumulation, will reinforce *Dand5* degradation, adding the second regulatory step[91,92]. DAND5 secretion on the right half of the node was shown to inhibit Nodal signalling[89]. After asymmetric *Dand5* expression is established, the left side of the node will no longer harbour a repressive Nodal environment, allowing for its expression on that half of the node. Soon after, and resulting from the leftward nodal flow, DAND5 molecules will start to accumulate on the left side. This will terminate Nodal signalling at the node, around E8.0[93]. Hence, DAND5 is responsible for both restriction of Nodal signalling to the left side of the embryo and terminating that signalling soon after.

Despite its short activation window, asymmetric Nodal signalling will be further reinforced and propagated to the left side of the embryo. This is possible due to Nodal's self-enhancement lateral inhibition system, that will maintain inhibition on the right side of the embryo, while strengthening the signal on the left half. In time, this activation will induce *Pitx2* expression[94] as well as left side gene expression[95,96], establishing the basis for a left-right (L-R) asymmetric body plan. Further studies using a knockout (KO) mouse model for *Dand5* showed that its correct asymmetric expression at the node is responsible for the establishment of the L-R asymmetry on the mouse embryo[89]. *Dand5* KO mouse displayed a randomization of the body plan, a situation called *situs ambiguus*, as well as significant rates of perinatal death (around 35%)[89].

The *Dand5* KO model helped understand that this gene plays a role in later stages of development, namely within cardiac development and independently of L-R asymmetry defects. The depletion of *Dand5* prolongs TGF-β/Nodal signalling in KO mouse hearts, which in turn leads to thickened left ventricular walls, in result of increased proliferation of cardiomyocytes during development[97]. In humans, an association between mutations in *DAND5* that decrease its antagonistic potential, laterality defects, and congenital heart diseases has been found[98]. The mechanism through which DAND5 influences heart development is still not totally clear.

Chapter 2 - Motivation and aims

DAND5 has been shown to be involved in the establishment of L-R asymmetry in both mice[89] and humans[98]. At the same time, it has been associated with cardiac development, with KO mouse showing thickened myocardial walls resulting from prolonged TGF-β signalling[97]. All these findings put DAND5 at the crossroads between several signalling pathways, Nodal/TGF-β, Notch, and Wnt, and within significant developmental contexts, such as cardiogenesis.

Taking advantage of the possibility of deriving mESCs from our *Dand5* KO mouse model, we aimed at understanding how the depletion of DAND5 would influence mESCs differentiation. To do so, we established a model of spontaneous differentiation, partially mimicking embryonic development. Since dissecting the *in vivo* phenotypes of our *Dand5* KO mouse model is not easy, we considered that an *in vitro* differentiation strategy could present significant advantages. The strategy to evaluate the role of DAND5 in mESC differentiation relied on assessing genetic expression changes between KO and WT cells. The data produced by such analysis served as guide for the different subsequent experiments.

Chapter 3 - Materials and Methods

3.1 Cell culture

Mouse embryonic stem cells (mESCs) were kept undifferentiated in 0.1% porcine gelatine (Sigma-Aldrich, USA) coated wells. *Dand5* KO mESCs were used to assess how the depletion of *Dand5* influences Embryoid Body (EB) differentiation, with E14 mESCs serving as wild type (WT) control. The derivation and primary culture of KO mESCs from blastocysts has been previously described[99]. Culture medium for pluripotency maintenance was KnockOut™ DMEM (Gibco, USA), containing 13.5% of Heat Inactivated HyClone Serum (GE Healthcare Life Sciences, USA), 1% of 200 mM L-glutamine (Gibco, USA), 1% of 10000 Units/ml Penicillin – 10000 µg/mL Streptomycin (Gibco, USA), 1% of 100X MEM Non-Essencial Amino acids (Gibco, USA), 0.2% of 50 mM β-Mercaptoetanol (Gibco, USA), supplemented with 0.1% of 10^6 Units/mL ESGRO® Leukemia inhibitory factor (Merk, Germany), 0.02% of 10 mM GSK-3 inhibitor IX (Calbiochem®, USA) and 0.008% of 50 mM PD98059 (MEK/ERK inhibitor) (Calbiochem®, USA). Cells were maintained in a humidified incubator at 37 ºC and 5% of CO_2. Culture medium was replenished every two days and passages were made when cells reached 80% confluency. To passage cells, culture medium was collected, cells were washed with Dulbelcco's phosphate-buffered

saline (DPBS) (Gibco, USA), and detached by incubating with calcium chelator TrypLE (Gibco, USA) for 5 minutes in a humidified incubator at 37 ºC and 5% of CO_2. TrypLE was then inactivated with culture medium, and cells were mechanically individualized. Cell suspensions were centrifuged at 1000 rpm for 5 minutes, using a centrifuge. Supernatant was then discarded, and cells were resuspended in culture medium. Using the new cell suspension, only 1:10 of cells were seeded onto new gelatine coated wells.

The day before EB formation was induced by the hanging drop method, culture medium was changed to medium without MEK and GSK-3 inhibitors. On day 0 of EB differentiation, cells were detached and dissociated as described above. After centrifugation and supernatant removal, cells were resuspended in culture medium without MEK/ERK, GSK-3 inhibitor, nor Leukemia inhibitory factor. Cells were counted and a cell suspension with 25 000 cells/mL was made. Using a multichannel micropipette, drops of 20 µL of cell suspension (500 cells per drop) were deposited on low adherence plates. Plates were then inverted, and 6 mL of DPBS were added to the lid, to maintain humidity. Plates were then incubated in a humidified incubator at 37 ºC and 5% of CO_2. On day 2 of differentiation, DPBS was discarded, plates were flipped, and 8 mL of culture medium (without inhibitors) were added to the drops. Growing EBs were kept in a humidified incubator at 37 ºC and 5% of CO_2. On day 4 of the protocol, half of the medium volume was replenished. At day 5, EBs were individually collected using

a micropipette and plated in gelatine coated wells. From that point on, EBs were kept in culture in a humidified incubator at 37 ºC and 5% of CO_2, until further use. The culture medium of plated EBs was replenished every two days.

3.2 RNA sequencing

For RNA sequencing (RNAseq) Total RNA was extracted from three biological replicates of WT and KO samples of mESCs, days 0, 5, 6, 8 and 10 of EB differentiation. Samples for each day were collected as previously describe and extraction was performed using AllPrep DNA/RNA/Protein (Qiagen, Germany), following the manufacturer's protocol for RNA extraction. Concentration and quality of samples were assessed using Nanodrop 2000 (Thermo Fisher Scientific, USA). Samples for each stage were pooled together, 2 ng per replicate. Libraries were constructed using Stranded mRNA Library Prep Kit. Pair-end libraries were sequenced on an Illumina PE150 Platform with an output of ~40 M reads per sample. The quality of the reads was assessed using FastQC software and mapping of reads was performed applying the STAR (version 2.7.5c) aligner using murine genome from GENCODE Release M25 as reference[100]. In particular, the primary genome sequence assembly GRCm38 together with corresponding annotations was used. To obtain the read counts per gene, the featureCount function of the Bioconductor package Rsubread (version 2.2.6) was executed[101]. As a measure of gene expression, the transcripts per million (TPM) and counts per million reads mapped (CPM) were subsequently

calculated. Finally, the analysis of differential gene expression was performed using Bioconductor edgeR package (version 3.30.3) with a biological coefficient of variation of 0.2[102]. P-value correction for multiple testing was performed using the Benjamini Hochberg (False Discovery Rate (FDR)) method. Mappings of Ensembl IDs to gene symbols were extracted from Bioconductor package org.Mm.eg.db for murine genome annotation (version 3.11.4). Principal Component Analysis (PCA) was conducted using the limma package[103]. Functional enrichment for Biological Process, Cell Compartment, and Molecular Function terms was done using an Over-Representation Analysis (ORA) approach, using differentially genes with FDR lower than 0.01, and conducted in WebGestalt[104]. The top 10 terms were selected. Functional enrichment analysis for KEGG pathway categories, ORA of differentially expressed genes (DEGs) was conducted using WebGestalt[104]. As input, DEGs with FDR lower than 0.01 and with either positive or negative logged (base 2) fold changes larger than 2 or smaller than −2 were selected. Using genes that associated with Heart

Cardiomyopathy and Dilated Cardiomyopathy terms of KEGG, a heat map was produced based on Z Scores, which were calculated by subtracting the overall average log2 TPM from the log2 TPM of the respective sample, dividing that result by the standard deviation of all log2 TPM values across all samples.

3.3 RNA isolation and complementary DNA synthesis

Table 3.1 - EB samples collected for RNA isolation

Day of EB differentiation	Samples collected
1	8 Petri dishes (around 70 EBs per Petri dish)
2	4 Petri dishes
3	2 Petri dishes
4	1 Petri dish
5	1 Petri dish
6	20 plated EBs
7	20 plated EBs
8	20 plated EBs

To assess genetic expression, RNA samples were collected every day of EB differentiation, up to day 8. The different samples collected can be seen on Table 3.1.

On day 0 of differentiation, mESCs not used for EB differentiation were lysed using TRI Reagent (Sigma-Aldrich, USA), and stored at -80 ºC for subsequent RNA extraction. For samples of days 1 and 2 of differentiation, when plates haven't been inverted and EBs are differentiating in drops, DPBS was used to collect EBs. The EB suspension was allowed to settle, and DPBS was discarded. TRI Reagent was then used to dissociate EBs. On days 3, 4, and 5, when EBs

were kept in suspension, medium containing EBs was collected, and they were allowed to settle down. Medium was then discarded, and TRI Reagent was then used to lyse cells. From day 6 onward, when EBs were plated, culture medium was discarded, and TRI Reagent was pippetted against the platted EBs to dissociate them. All these RNA samples were stored at -80 ºC until further processing. The volume of TRI Reagent used to lyse all samples was 200 µL. After all samples were collected, they were taken out of -80 ºC storage and put in ice. Then, RNA was extracted using Direct-zol RNA Miniprep Kit (Zymo Research, USA), according to manufacturer's instructions, using 30 µL of DNase/RNase-Free water for the final elution step. Sample's concentration and quality were assessed using Nanodrop 2000 (Thermo Fisher Scientific, USA). For complementary DNA (cDNA) synthesis 1000 ng of RNA were used. The reaction mix was done using Oligo dT Primer, RiboLock RNase Inhibitor, RevertAid Reverse Transcriptase, and dNTPs (Thermo Fisher Scientific, USA). cDNA synthesis was set up following manufacturer's instructions. These reactions were set up in a thermocycler (C1000 Thermal Cycler, Bio-Rad), with the following reaction steps: 60 ºC for 5 min, 42 ºC for 1 h, 70 ºC for 5 min. Initially, only solutions of cDNA and Oligo dT Primer were introduced in the thermocycler. After the first step, the remaining reagents were added to the reaction mix. Final solutions were diluted 1:10 using DNase/RNase-Free water and stored at -20 ºC until further use.

3.4 Real time quantitative PCR experiments

Reaction mixes for real time quantitative PCR (RT-qPCR) were done according to Table 3.2, and the primers used are listed on

Table 3.3. Reactions were run in QuantStudio™ 5 Real-Time PCR system (Applied Biosystems™, USA). The reaction steps are the following: denaturation of cDNA chains at 95 ºC for 2 min, 40 cycles of denaturation step (95 ºC) for 10 s, annealing for 20 s, extension at 72 ºC for 20 s. Annealing temperatures can be consulted on

Table 3.3. Fold changes were calculated using the $2^{-\Delta\Delta CT}$ method[105], using *Pgk1* and *Gapdh* as reference genes. Three technical replicates were used for each sample.

Table 3.2 - RT-qPCR reaction mix

	1 replicate (µL)
SensiFAST™ SYBR® Lo-ROX (Meridian Bioscience, USA)	7.5
DNase/RNase-Free Water (Thermo Fisher Scientific, USA)	3.5

Forward Primer	1
Reverse Primer	1
cDNA	2
Total volume	15

Table 3.3 - Primers used on RT-qPCR reactions

Gene	Forward (5' – 3')	Reverse (5' – 3')	Annealing Temp. (ºC)
Gaphd	GGGAAGCCCATCACCATCTTC	AGAGGGGCCATCCAAGTCT	61 ºC
Pgk1	ATGGATGAGGTGGTGAAAGC	CAGTGCTCACATGGCTGACT	58 ºC
Snai1	GCCTGGGCGCTCTGAAG	AGGCCTGGCACTGGTATCTCT	67 ºC
Snai2	TATGCTGCCTTCCAGGCTTG	TATGCTGCCTTCCAGGCTTG	62.9 ºC
Twist1	TATGCTGCCTTCCAGGCTTG	TATGCTGCCTTCCAGGCTTG	69 ºC
Cdh1	TCTACCACGTCCACAGTGAC	CCAGCAGTTCGTTGTTGTCA	62.5 ºC
Cdh2	GGATGAAACGGCGGGATAAA	TCTTCTTCTCCTCCACCTTCTT	62.9 ºC
EpCAM	GCTGGCAACAAGTTGCTCTCTGAA	CGTTGCACTGCTTGGCTTTGAAGA	62.5 ºC
Prickle	CAAGCCTCGGTGCTCAGC	GATATATCTCTGCCCTCCCAGG	67.2 ºC

3.5 EB spreading measurement

At day 5 of differentiation, EBs were plated in gelatine coated wells and maintained in a humidified incubator at 37 ºC and 5% of CO_2. Starting at 12 h post

platting, EBs were photographed every 12 h using a transmitted light inverted microscope (EVOS™ XL, Thermo Fisher Scientific, USA). Images were then processed using Fiji[106], by drawing the EB spreading perimeter and measuring the respective ROI area. Spreading rates were calculated by dividing the given area by the spreading area at 12 h of the given EB. Statistical analyses were performed using GraphPad Prism version 8.2.1 for Mac OS (GraphPad Software, USA).

3.6 Migration experiments

At day 5 of differentiation, EBs were dissociated, cells were counted and 2×10^5 cells were seeded per well of a 24-well tissue culture plates (TPP, Switzerland). Cells were monitored for confluence, which was usually reached 24 h after dissociation. At that time, they were mitotically inactivated using cell culture medium supplemented with 10 µg/mL of Mitomycin C (Sigma-Aldrich, USA) in culture medium for 2 h. After that, cells were washed with DPBS three times before replenishing the culture medium.

A scratch was then made using a micropipette tip. To remove cell debris, cells were gently washed with DPBS before adding cell culture medium and imaging. To assure that the photos were always made in the same location, two places on each well were marked, and pictures were taken. Wound healing

assessment was done every 2 h, up to 8 h, moment at which WT cells had closed the scratch area.

Images were then processed using Fiji[106]. Scratch areas were drawn, and the respective Regions of Interest were saved. Using these, the areas were measured, and the wound closure rate was calculated by dividing the area at a given time point by the respective initial area. Statistical analyses were performed using GraphPad Prism version 8.2.1 for Mac OS (GraphPad Software, USA), multiple paired *t-tests* were performed and *p*-value < 0.05 was considered statistically significant.

3.7 EB staining

EBs at day 5 of differentiation were plated onto 0.1% porcine gelatine coated glass cover slips. Until collection day, culture medium was replenished every two days. Medium was then discarded, and cells were fixed in 4% Parafolmaldehyde (PFA) (Sigma-Aldrich, USA) and 0.5% Triton X-100 (Sigma-Aldrich, USA) for 15 min at room temperature (RT). Fixative solution was then removed, and cells were permeabilized with DPBS + 0.1% Triton X-100 for 30 min at RT. After permeabilization, blocking was done using blocking solution (100 mM Glycine (Sigma-Aldrich, USA), 2% (w/v) Bovine Serum Albumin (BSA) (NZYTech, Portugal), 3 mM Sodium Azide (Merk, Germany), in DPBS), incubating 2 h at RT.

After blocking, samples were incubated with the primary antibody (see Table 3.4.) overnight (O/N) at 4 ºC. Samples were then washed 3 times with DPBS + 0.1% Triton for 10 min at RT. The respective secondary fluorophores were then added to samples and incubated for 2 h at RT in the dark. After that, samples were washed 2 times with DPBS + 0.1% Triton for 10 min, and once with DPBS for 10 min at RT. Finally, nuclei were stained for DAPI (Santa Cruz Biotechnology, USA) (1:100 dilution in DPBS), for 10 min at RT. Samples were mounted onto glass microscope slides using Vectashield (Vector Laboratories, USA) as mounting medium. Samples were stored at 4 ºC in the dark until further use. Multichannel immunofluorescence images were obtained using a Zeiss LSM980 confocal microscope (Zeiss, Germany).

3.8 Focal adhesions quantification

The immunofluorescence protocol was carried on using αVinculin, Phalloidin and DAPI. EBs were imaged using a confocal microscopy. The images were taken using a Z-Project method that was able to image the areas below and above the FA level. Image Processing protocol was reproduced from Nardone *et al.*, 2017[107], and provided us data on FA number and FA area. Normalization of those values was done by dividing those values by the cell coverage area. All image processing steps were done using Fiji[106]. Statistical analysis was performed using GraphPad Prism version 8.2.1 for Mac OS, unpaired *t-test* was done and *p*-value < 0.05 was considered statistically significant.

3.9 Animals

The animals used in this work were kept at 21 ºC in a 12 h light-dark cycle. Experiments were conducted according to European Union guidelines for animal research and welfare, as well as in compliance with the Portuguese law. The project was approved by the Consultative Commission of the Veterinary Agency from Portuguese Ministry of Agriculture (Directive 2010/10/63/EU of the European Parliament). Experiments were conducted under DGAV Permit No. 0421/000/000/2016.

Both mouse lines used in this work are in 129 genetic background. The *Dand5* KO mouse line was previously generated using E14 stem cells[89]. Timed pregnancies were established, and noon of the plug detection day was considered E0.5. At E11.5, pregnant females were sacrificed using CO_2 and subsequent cervical dislocation. An abdominal incision was made, and the abdominal cavity exposed. Uterine horns containing the embryos were dissected and stored in cold DPBS.

3.10 Paraffin embedding and sectioning

Freshly collected individual embryos at E11.5 in cold DPBS were dissected and fixed in 4% PFA + 0.5% Triton X-100 for 2 h at 4 ºC. After fixation, embryos were washed 3 times with DPBS for 10 min at RT, in order to clear residual PFA. Embryos were then dehydrated through a Methanol (Honeywell, Germany)

gradient (25%, 50%, 75%, 100% in DPBS), 20 min in each solution. Incubation in 100% Methanol was repeated once more, and embryos were then stored at -20 ºC O/N.

The next day, embryos were allowed warm up to RT for around 1 h. They were then incubated in a 1:1 solution of Xylene (VWR, USA) and 100% Methanol, for 15 min at RT with light agitation. Afterwards, embryos were washed in Xylene 2 times. The first wash lasted until embryos became transparent, point at which Xylene was replenished, before being finally discarded. Melted paraffin (Sigma-Aldrich, USA) was then added to the samples and incubated for 30 min at 60 ºC. Three 20 min washes with fresh melted paraffin were then done, before placing the embryos in a paraffin mould for subsequent sectioning. Embryos were placed facing down, in order to obtain coronal sections. Samples in paraffin were allowed to solidify for 1 h at RT. Using a Ergostar HM 200 (Microm International, Germany) microtome, samples were first trimmed and, upon reaching the heart region, 7 µm sections were obtained. Ribbons of sections were placed in Superfrost™ Plus (Thermo Fisher Scientific, USA) and dried at 37 ºC O/N. Sections were then stored at 4 ºC until further use.

3.11 Staining of paraffin sections

Sections were chosen and incubated briefly at 70 ºC. Paraffin was then removed by washing slides in Xylene (three 5 min washes at RT). Samples were

rehydrated using an Ethanol gradient (3 min in each solution at RT): two washes in 100% Ethanol, one wash in 90%, 70% and 50% Ethanol. Slides were then rinsed in distilled water.

Antigen retrieval was performed by microwaving slides in Citrate Buffer pH 6 (1 mM Tri-Sodium Citrate (Sigma-Aldrich) and 0.5% Triton X-100) for 30 min. Samples were allowed to cool down at RT before being washed with DPBS + 0.1% Triton X-100 (three 5 min washes at RT). A blocking step followed, incubating samples with blocking solution (2% BSA and 0.1% Triton X-100, in DPBS) for 2 h at RT. Primary antibody solution was then added to slides, and incubated O/N at 4 ºC, in a humid atmosphere, protected from light. The next day, slides were washed three times with DPBS + 0.1% Triton X-100, for 5 min at RT each. Secondary antibody was then added and incubated for 2 h at RT, protected from light. Slides were washed two times with DPBS + 0.1% Triton X-100 and one time with DPBS, for 5 min each washing step. Nuclei were then stained using 1:100 DAPI solution. Finally, slides were washed two times with DPBS, for 5 min each wash, and mounted using Vectashield mounting medium. The antibodies used can be consulted in Table 3.4.

Table 3.4 - List of antibodies

Antibody	Brand / Catalogue Number	Dilution used	Method
α-Vinculin	Sigma-Aldrich, V9131	1:500	EB staining

Alexa Fluor™ 647 Phalloidin	Thermo Fisher,	1:500	EB staining
α-pSMAD	Cell Signalling, 3174	1:100	Paraffin sections staining
α -ISL1	DSHB, 39.4D5	1:200	Paraffin sections staining

3.12 OCT embedding and sectioning

For LacZ β-Galactosidase staining, embryos collected at E11.5 were used. Samples were fixed in 4% PFA + 0.5% Triton X-100 for 2 h at 4 ºC. Samples were washed 3 times in DPBS for 10 min at 4 ºC, and then dehydrated with a D(+)-Sucrose (Sigma-Aldrich, USA) gradient. Samples were incubated in 10% and 20% Sucrose solutions for 1 h at 4 ºC. Finally, embryos were placed in 30% Sucrose O/N at 4 ºC. Embryos were placed in OCT moulds and residual Sacarose was removed. OCT (VWR, USA) was added to the mould and embryos were placed facing down and slowly frozen using ice and then placing samples at -20 ºC. Using a cryostat (Leica CM3050 S, Leica, Germany), sections with 10 µm of thickness were obtained, and the ones with the heart region were selected.

3.13 Staining of OCT sections

Slides with sections containing the heart region were selected for LacZ β-Galactosidase staining. They were allowed to reach RT and then were washed

with DPBS for 10 min. The slides were then washed with Salmon-Gal wash solution (0.01 % (w/v) Sodium deoxycholate (Merk, USA), 0.02% (v/v) NP-40 (Merk, USA), 2 mM $MgCl_2$ (Merk, USA), in DPBS), three washes of 20 min. Samples were then incubated with staining solution (1 mg/mL Red-Gal (GERBU Biotechnik, Germany), 0.33 mg/mL 4-Nitro blue tetrazolium chloride (Roche, Switzerland) in Salmon-Gal wash solution) at 37 ºC in a humid closed container, protected from light. Staining incubation was done until staining became visible, which happened after about 3 days, with staining solution being changed every 48 h. At that point, staining solution was washed with DPBS, and cover slips were mounted using DPX mountant (Sigma-Aldrich, USA). Brightfield images were obtained using a Zeiss Axio Imager.Z2 microscope (Zeiss, Germany).

Chapter 4 - Depletion of *Dand5* during embryoid body differentiation enhances cardiac genes expression, while disrupting Wnt and Notch pathways

Part of the results on this chapter were published on:

Inácio JM, **von Gilsa Lopes J**, Silva AM, Cristo F, Marques S, Futschik ME and Belo JA (2021) DAND5 Inactivation Enhances Cardiac Differentiation in Mouse Embryonic Stem Cells. *Front. Cell Dev. Biol.* 9:629430. doi: 10.3389/fcell.2021.629430

4.1 Introduction

EB differentiation allows easy, spontaneous, and easily scalable differentiation of mESCs. At the same time, this differentiation strategy allows the obtention of cells of all three germ layers, while partially resembling embryonic development[108–110].

To understand how the depletion of *Dand5* influences EB differentiation, we used mESCs derived from blastocyst cells of *Dand5* KO mouse model, in which the second exon had been replaced by a neomycin and lacZ cassette[97]. These cells were tested for pluripotency and differentiation markers, and their karyotype was confirmed before EB experiments[99]. Using these cells, we have reported an increase in cardiomyocyte differentiation during EB differentiation, resulting from earlier expression of cardiac genes and higher proliferation rates in KO cells[99]. Figure 4.1 details some of those results, showing the quantitative differences in beating foci (Figure 4.1 A) and cardiac progenitors (Figure 4.1 B). We also were able to show improved organisation and maturation of cardiac cells in EBs at day 6 of differentiation (Figure 4.1 C).

Considering EB differentiation as a model for embryonic development, we designed a RNAseq analysis experiment to evaluate how the depletion of *Dand5* impacted not only cardiogenesis, but also another developmental pathways. Namely, we collected RNA of the initial mESC, then we collected RNA at days 5,

6, 8, and 10 of differentiation (a schematic can be seen on Figure 4.2 A). Day 5 of differentiation directly precedes EB plating, and when cells are entering EMT. Samples at day 6 were collected 24 h after platting, to assess the effect of platting and attachment on genetic expression. The emergence of cardiac features in KO EBs around days 6 and 7 of differentiation led us to choose two late time points for assessment of cardiac genes expression.

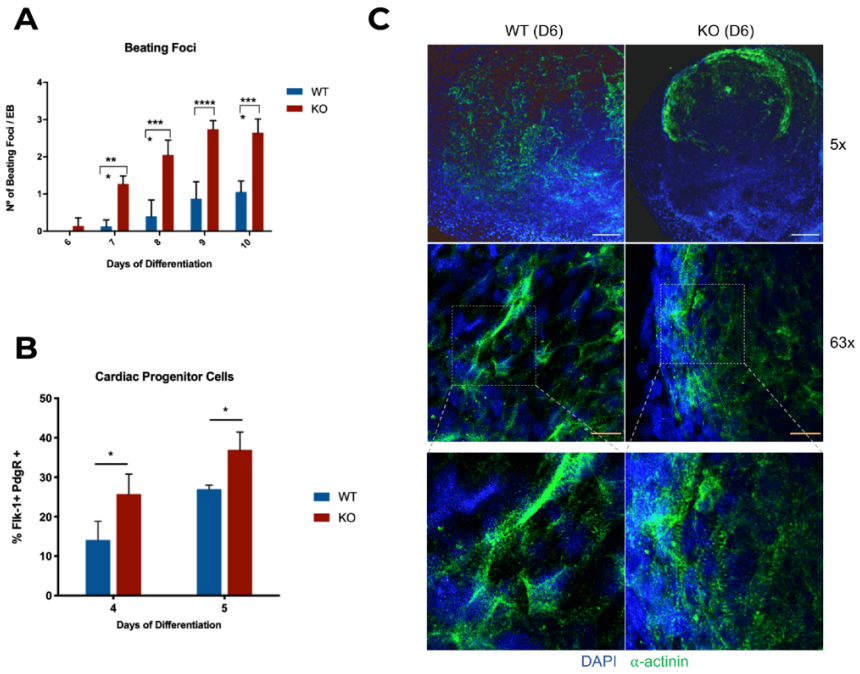

Figure 4.1 – Enhancement of cardiac features in KO EBs (adapted from Inácio, J., 2021). A) Measurement of beating foci in WT and KO EBs; B) Flow cytometry analysis of FLK-1 and PDGFR-α expression in EB cells; C) WT and KO EB immunofluescence staining for α-actinin at day 6 of differentiation (scale bars: white 200 μm; yellow 20 μm).

In this chapter, we present the RNAseq analysis results, focusing on changes in signalling pathways and cell-specific marker genes.

4.2 Results

4.2.1 The depletion of *Dand5* during EB differentiation speeds up cellular transitions

A schematic for the RNAseq experiment design can be seen on Figure 4.2 A, detailing EB differentiation hallmarks and the time points at which sample were collected. The results for the PCA can be seen in Figure 4.2 B. Initial samples, pluripotent mESCs, are located closely together, as they have yet to exit pluripotency. As for samples from day 5 to day 8, the PCA shows that there is a shift in their temporal evolution, with KO samples closer to WT samples of later stages. This clustering pattern suggests that *Dand5* KO EBs progress faster through differentiation. Next, we decided to confirm the existence of different expression patterns upon depletion of DAND5 during EB differentiation on a gene level (Figure 4.2 C). We obtained an overall picture of genetic expression across the time series by visualization and clustering of the DEGs that were detected on our dataset. As the resulting heat map on Figure 4.2 C displays, expression patterns of *Dand5* KO samples are distinct from their WT counterparts, mainly at days 5, 6 and 8. Differences can still be observed on day 10 samples, but not in the same degree as in the other days, which is in accordance with the PCA (Figure 4.2 B). Euclidean clustering of the samples, according to their genetic expression

pattern is depicted on Figure 4.2 C. Once more, we can see that KO samples are closer together at days 5 and 6, when EBs are platted and start developing cardiac features, such as beating foci.

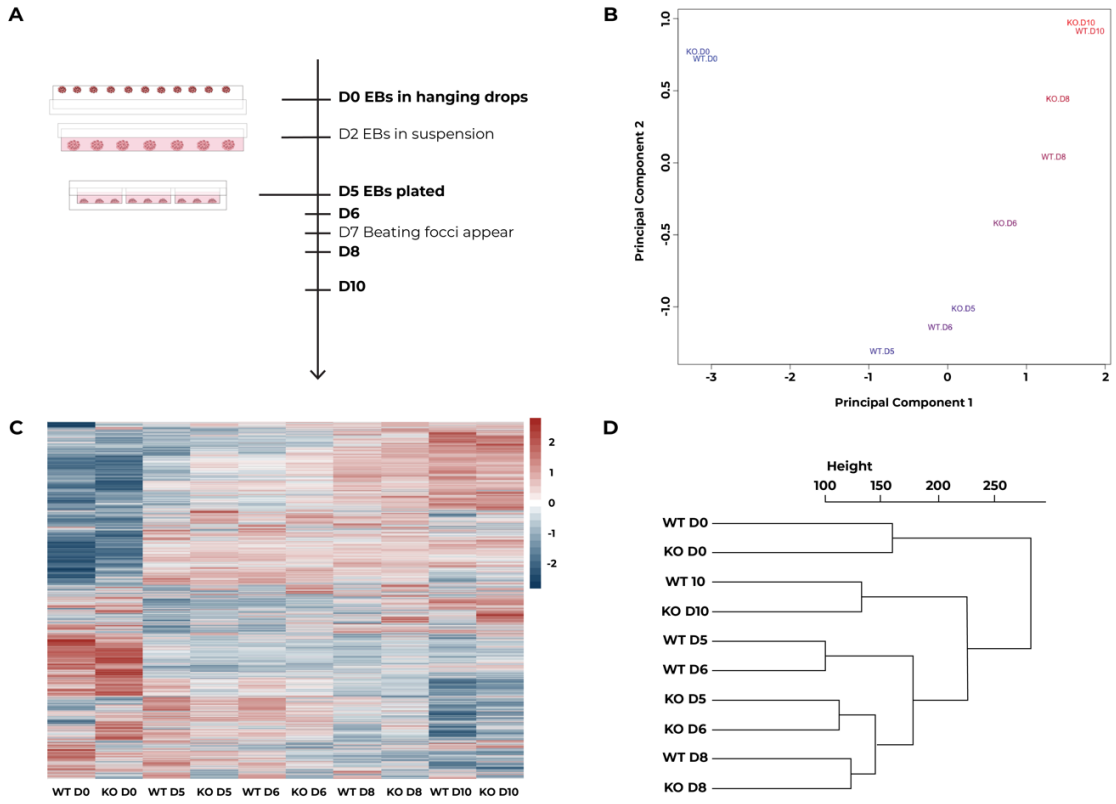

Figure 4.2 - Schematic representation of RNAseq experiment, with EB differentiation hallmarks. Days in bold represent timepoints at which RNA samples were collected; B) Principal component analysis result; C) Heatmap for all differentially expressed genes (DEGs), representing differential expression in KO vs WT samples; D) Euclidean clustering of samples according to the respective DEGs

4.2.2 Genetic expression in *Dand5* KO EBs shows a different pattern concerning main developmental signalling pathways, as well as membrane proteins

Using all the DEGs, we conducted an ORA for each of the days of our dataset searching for the top 10 Gene Ontology (GO) terms regarding molecular function (MF), biological process (BP), and cell compartment (CC). We also conducted ORA for regulatory differences in pathways. For this last type of analysis, we divided the input genes according whether they were upregulated or downregulated, to understand which pathways might be induced/repressed.

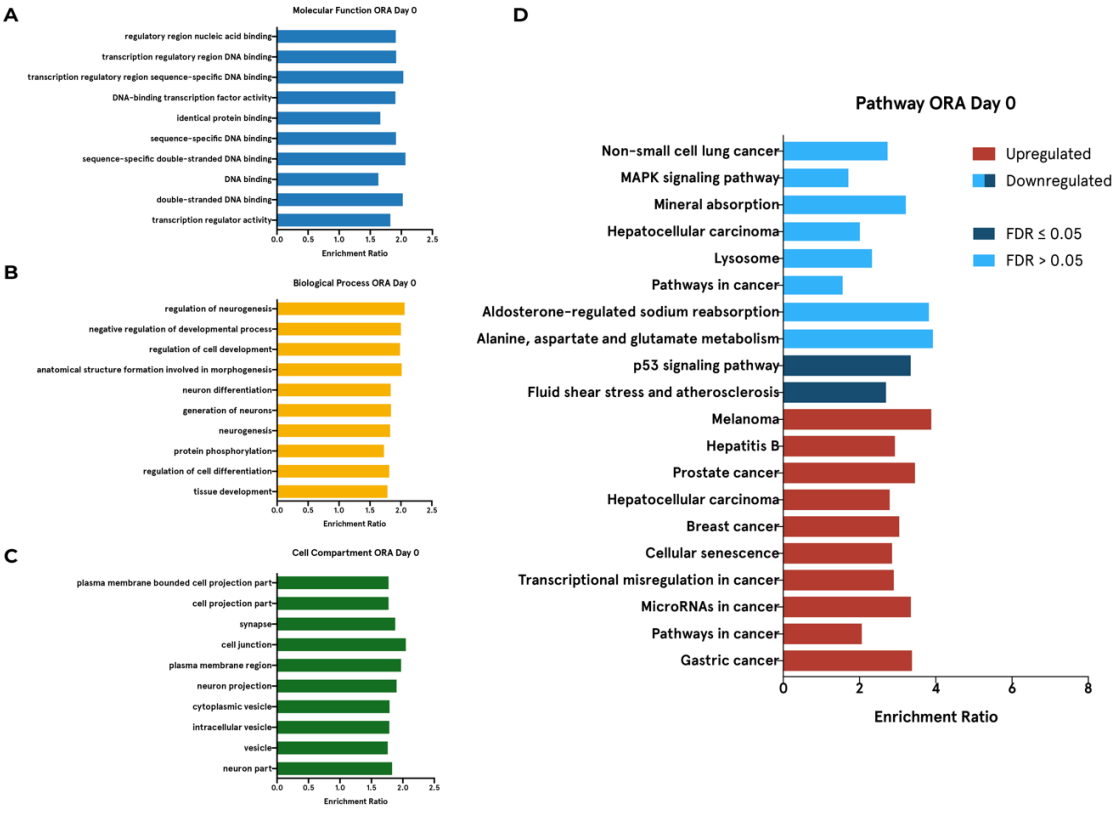

Figure 4.3 - Over-Representation Analysis results at day 0 of differentiation; A) Molecular function GO terms; (all terms with FDR ≤ 0.05) B) Biological process GO terms (all terms with FDR ≤ 0.05); C) Cell compartment GO terms (all terms with FDR ≤ 0.05); D) Pathway GO terms (all terms with FDR ≤ 0.05, except when indicated otherwise by bar color). (GO – Gene Ontology; FDR – False Discovery Rate)

The results for day 0 can be seen on Figure 4.3. As for the results on MF (Figure 4.3 A), we can observe that the GO terms are mostly related with DNA binding and TF activity. This agrees with BP results, on Figure 4.3 B, that show that the genes differentially expressed are mainly related with differentiation processes, particularly with neural differentiation. Lastly, DEGs of CC ORA terms at day 0 are encode proteins located at cell projections, cell junctions, and neuronal cells structures.

The results of ORA for Pathway GO terms can be seen on Figure 4.3 D. From all the downregulated GO pathway terms, only two display significant FDR values. Upon closer inspection of the resulting Kyoto Encyclopaedia of Genes and Genomes (KEGG) maps, we can observe that, for the “fluid shear stress and atherosclerosis” (KEGG entry mmu054189), most downregulated genes encode membrane proteins (e.g., *Itgb3*, an integrin, *Tnfrsf1a*, a membrane receptor, *Icam1*, a cell-cell adhesion molecule). As for the “p53 signalling pathway” term (KEGG entry mmu04115), some of the downregulated genes are related with cell cycle, such as *Cdkn2a*, a cyclin, DNA repair and damage prevention (e.g., *Sesn3* or two Gadd45, Growth Arrest and DNA Damage, genes). Regarding upregulated pathways, a significant number of terms are related to cancer. Using the respective KEGG maps to understand these results, we could see that the dysregulated genes are mostly related with cell cycle (e.g., *Ccnd1*, *Ccne1*, cyclins, *Cdkn2a*, a cyclin dependent kinase inhibitor).

The results of ORA for Day 5 of EB differentiation can be seen on Figure 4.4. There is a considerable similarity with the results from day 0, on Figure 4.3 A, namely the ones concerning DNA-binding. Compared with the results for MF on day 0 (Figure 4.3 A), there is a clear difference in terms of enrichment ratio for the “extracellular matrix structural constituent” term. This value, which is conveys the overlap between DEGs of the dataset and genes of the GO term, is more than double the value of the other enriched terms. Upon closer inspection, most of the genes overlapping with this GO term are Collagen or Laminin subunits. As for the BP and CC terms, these results are similar to the ones for day 0 (Figure 4.3 B and C), related with neural differentiation, axons, and plasma membrane. The results on Figure 4.4 D show the GO pathway terms obtained in the ORA. Among the downregulated terms, significant terms with low FDR values include terms related with cancer. The genes overlapping with those sets are related with different pathways (e.g., Wnt pathway genes: *Wnt8a* or *Wnt3a*; FGF pathway genes: *Fgf5* or *Fgf4*; Notch pathway genes: *Notch1* or *Jag1*). Following these results, GO terms related with Wnt and Notch signalling pathways are also downregulated, but only the latter has a FDR value below 0.05, meaning that the upregulation of the Notch term is statistically significant. It is also important to highlight the presence of “Cell adhesion molecules” in the downregulated terms, which is in agreement with MF and CC ORA results for the same day. Among the overlapping genes, we can find cadherins (*Cdh4* and *Cdh2*), an integrin subunit (*Itga6*), or

genes encoding neuronal cells adhesion proteins (*Nrcam*, *Nfasc*, *Nrxn1* and *Nrxn2*). Upregulated terms also show that EB cells have progressed through differentiation, and we see once more that several pathways are upregulated, such as Rap1, PI3K-Akt or Relaxin. Furthermore, the upregulation of "Hypertrophic cardiomyopathy" and "Dilated cardiomyopathy" reveals that KO cells have already entered cardiac differentiation by day 5. Genes overlapping with these GO sets encode membrane proteins, such as integrins, or cardiac sarcomere components, such as troponin and myosin. There are also terms that

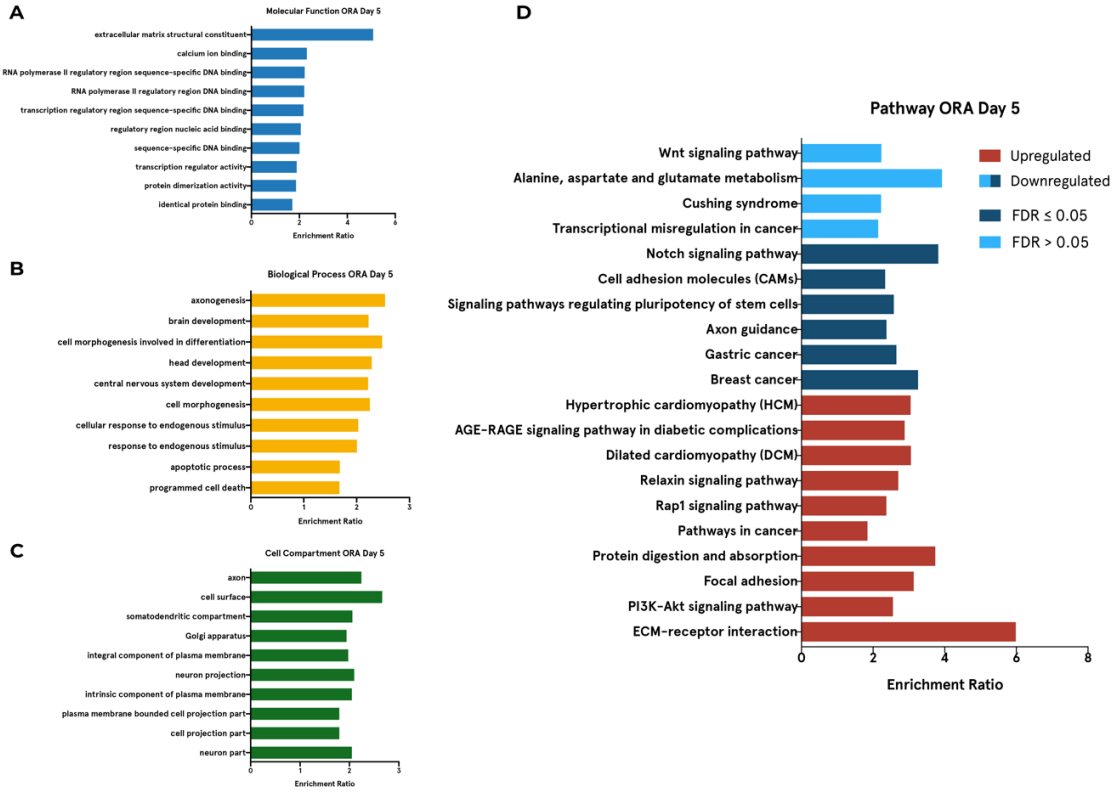

Figure 4.4 - Over-Representation Analysis results at day 5 of differentiation; A) Molecular function GO terms (all terms with FDR ≤ 0.05); B) Biological process GO terms (all terms with FDR ≤ 0.05); C) Cell compartment GO terms (all terms with FDR ≤ 0.05); D) Pathway GO terms (all terms with FDR ≤ 0.05, except when indicated otherwise by bar color)

follow the results related with cell membrane and ECM components from Figure 4.3 A and C, such as “ECM-receptor interaction”, that comprises genes encoding subunits of collagen and laminin.

ORA of DEGs at day 6 can be seen on Figure 4.5. Similarly to day 5 results, the enriched MF terms (Figure 4.5 A) are mostly related with DNA binding and TF regulation, and the most enriched term is related with ECM content. The top 10 BP terms present a contrast to the ones from the preceding day (see Figure 4.5 B). In this case, the terms related with axon and neural development are not present, except for “head development”. Instead, genes differentially expressed at day 6 overlap with gene sets pertaining to muscle tissue development, embryonic organ development, angiogenesis, and heart morphogenesis. On the CC ORA (Figure 4.5 C), most significant terms are still related with cell membrane and surface, as well as cell junctions. Finally, on Figure 4.5 D, we can observe the downregulation of terms mostly related with cancer. Upon further exploring these results, we see that most of the genes overlapping encode Wnt pathway molecules (e.g., *Wnt3* or *Wnt5a*), Notch ligands (e.g., *Dll1* or *Dll3*), and FGF pathway (e.g., *Fgf10* and *Fgf8*). Moreover, at day 6, we also see the downregulation of terms related with Wnt signalling pathways. Closer inspection of the KEGG maps for the Wnt term revealed DEGs encoding canonical Wnt ligands, such as *Wnt3* or *Wnt9b*, Wnt/Ca^{2+} activating ligands, *Wnt5a* and *Wnt5*, inhibitors, such as *Dkk1* and *Notum*, or even cellular signalling transducers like

Axin2 or *Lef1*. The upregulated pathway GO terms at day 6 of EB differentiation show that KO EBs also express a higher number of cardiac genes at this stage. Moreover, terms related with ECM and FAs are also enriched in these results.

Moving on the EB differentiation timeline, the results for the different ORA analysis at day 8 of differentiation can be seen on Figure 4.6. MF results, on Figure 4.6 A, follow the trend of the other days of EB, with terms related with DNA binding, TF regulation, and genetic expression coming up. The results for BP

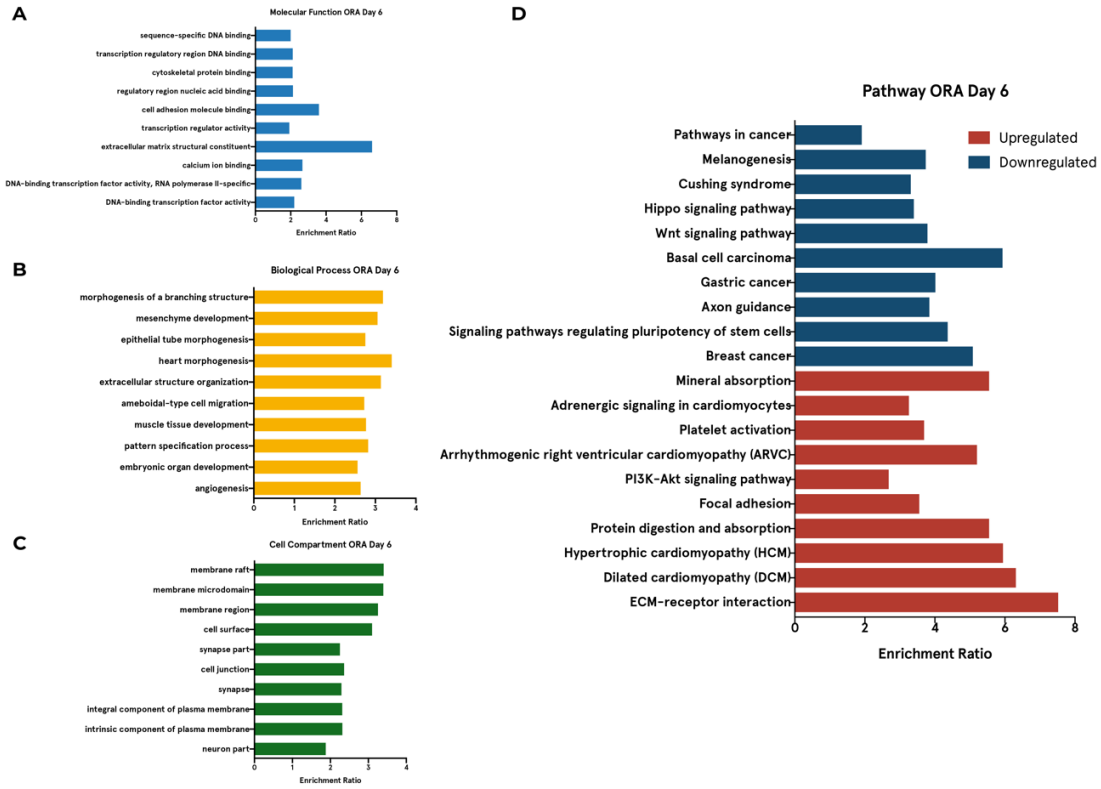

Figure 4.5 - Over-Representation Analysis results at day 6 of differentiation; A) Molecular function GO terms (all terms with FDR ≤ 0.05); B) Biological process GO terms (all terms with FDR ≤ 0.05); C) Cell compartment GO terms (all terms with FDR ≤ 0.05); D) Pathway GO terms (all terms with FDR ≤ 0.05)

ORA, on Figure 4.6 B, show once more that DEGs on day 8 are related with morphogenesis and neuronal differentiation, similarly to the results from days 0 and 6, on Figure 4.3 B and Figure 4.5 B, respectively. The results for CC ORA of genetic expression at day 8 can be seen on Figure 4.6 C, showing significant enrichment for terms related with plasma membrane and extracellular matrix.

Lastly, the Pathway ORA results are on Figure 4.6 D. Only one of the downregulated terms displays a significant FDR, “Transcriptional misregulation in

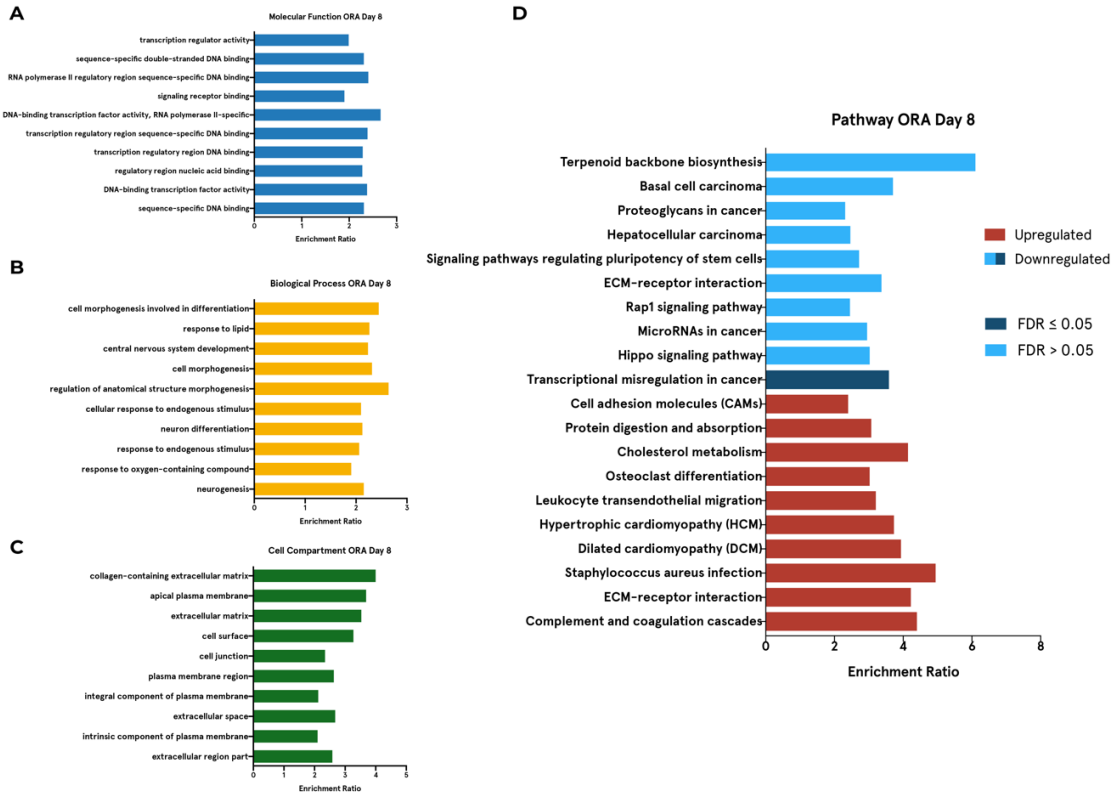

Figure 4.6 - Over-Representation Analysis results at day 8 of differentiation; A) Molecular function GO terms (all terms with FDR ≤ 0.05); B) Biological process GO terms (all terms with FDR ≤ 0.05); C) Cell compartment GO terms (all terms with FDR ≤ 0.05); D) Pathway GO terms (all terms with FDR ≤ 0.05, except when indicated otherwise by bar color)

cancer". From the respective KEGG map (KEGG entry mmu05202), the genes overlapping with the GO term are related with differentiation resistance (e.g., *Hoxa9*, *Meis1*, or *Fut8*) and angiogenesis (*Pax7* and *Pax3*). Among the high-FDR terms, terms such as "ECM-receptor interaction", "Hippo signalling pathway", or "Rap1 signalling pathway" are highlighter. The upregulated terms show that dysregulated genes are altering the way cells adhere to their microenvironment and other cells ("Cell adhesion molecules" and "ECM-receptor interaction" terms), while promoting cardiac differentiation ("Hypertrophic cardiomyopathy" and "Dilated cardiomyopathy" terms).

For the last day of EB differentiation analysed, day 10, ORA results can be seen on Figure 4.7. MF results point towards genes encoding ECM components, as well as cell adhesion molecules. These results also show that DEGs at this point are still associated with TF and DNA binding (Figure 4.7 A). As for BP terms, on Figure 4.7 B, once more we can see terms related with morphogenesis and neuronal differentiation, while CC terms agree with the ones regarding MF. Figure 4.7 C shows that the top 10 CC terms are related with the extracellular environment and cell membrane. Finally, Pathway ORA results, on Figure 4.7 D, show that KO EBs are repressing cardiac genes, as well as ECM and FA related terms. On the other hand, upon inspecting the KEGG maps for the upregulated terms, genes encoding integrin subunits, Wnt ligands (e.g., *Wnt7b* or *Wnt10b*)

and receptors (e.g., *Fzd5* or *Fzd6*), or TJ components such as *Cldn6* or *Cldn7* were detected.

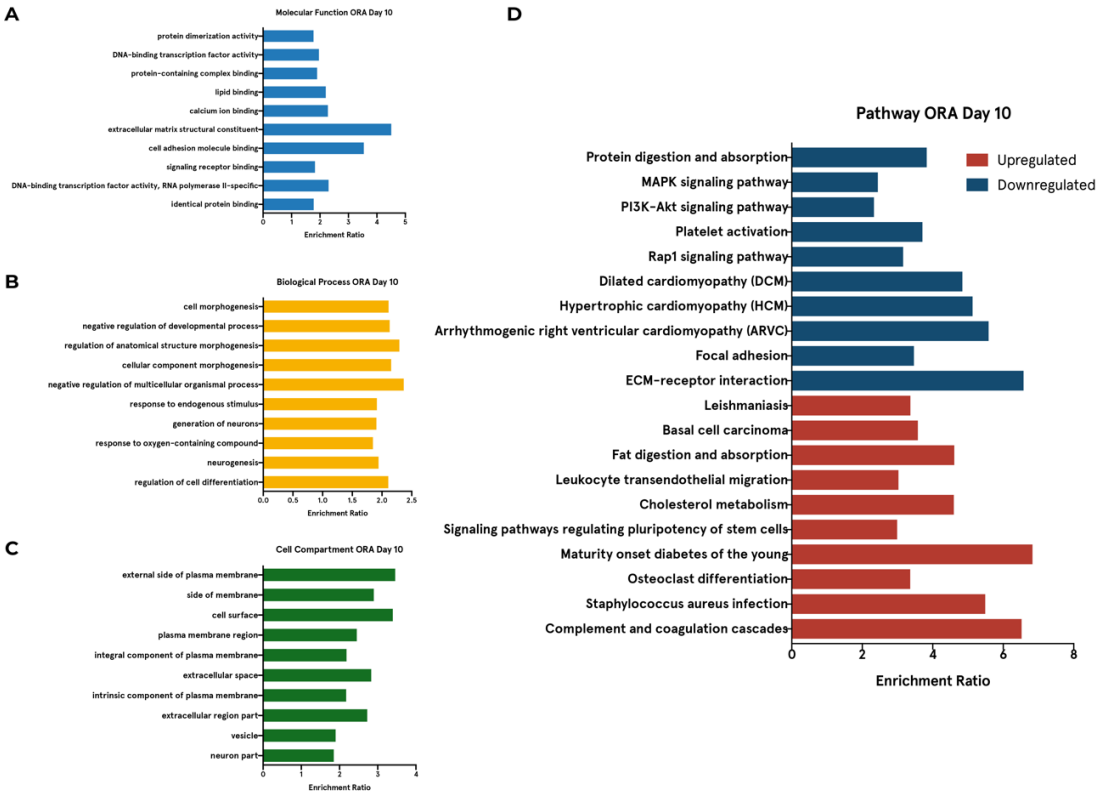

Figure 4.7 - Over-Representation Analysis results at day 10 of differentiation; A) Molecular function GO terms (all terms with FDR ≤ 0.05); B) Biological process GO terms (all terms with FDR ≤ 0.05); C) Cell compartment GO terms (all terms with FDR ≤ 0.05); D) Pathway GO terms (all terms with FDR ≤ 0.05)

4.2.3 Cardiac differentiation is heightened in KO EBs

The next logical step was to investigate whether the KO of *Dand5* in EB differentiation had any effect on cardiomyocyte differentiation, following previous reports of hyperplasia of the LV in *Dand5* KO mice and the results of the ORA,

detailed in the previous section, that showed genetic expression changes related with cardiac differentiation.

To do so, we gathered the DEGs that overlapped with GO terms related with the cardiac system, namely “Hypertrophic cardiomyopathy” and “Dilated cardiomyopathy”. A heat map of the expression of those genes can be seen in Figure 4.8. Several genetic expression trends are noticeable throughout the EB differentiation process. There is a considerable number of genes that start to be upregulated on KO samples at day 5 of differentiation, the ones in the lower half of the heat map. These genes encode proteins that will form calcium channels (e.g., *Cacnb2* or *Cacna1d*), integrin subunits (e.g., *Itga4*, *Itga1*, or *Itga2b*), and even proteins that will form sarcomeres, such as *Tnnc1* or *Tnnt2*. We can also distinguish a group of genes that are upregulated on KO cells at later time points, starting at day 6. In this group we find genes encoding cardiac sarcomere proteins, such as *Mybpc3*, *Myh6*, or *Ttn*, as well as genes encoding integrin subunits (e.g., *Itga3* or *Itga7*). Apart from these two groups of genes, we can observe some genes that are upregulated earlier in the differentiation process, then downregulated, and are once again more expressed in WT samples at later stages (e.g., *Itga6* or *Itga4*). Furthermore, there are two genes, *Cacna2d2* and *Tnf*, which are consistently upregulated in WT samples from day 5 onwards.

The heat map on Figure 4.8 shows an overall picture of the genetic expression of cardiac genes, it does not detail their levels of expression, nor does

it allow for a comparison between genes, since the Z-score used to establish colours only normalizes expression for each row. To understand better the different levels of expression of these genes, we investigated their counts per million (CPM), which allows comparing expression profiles of different genes.

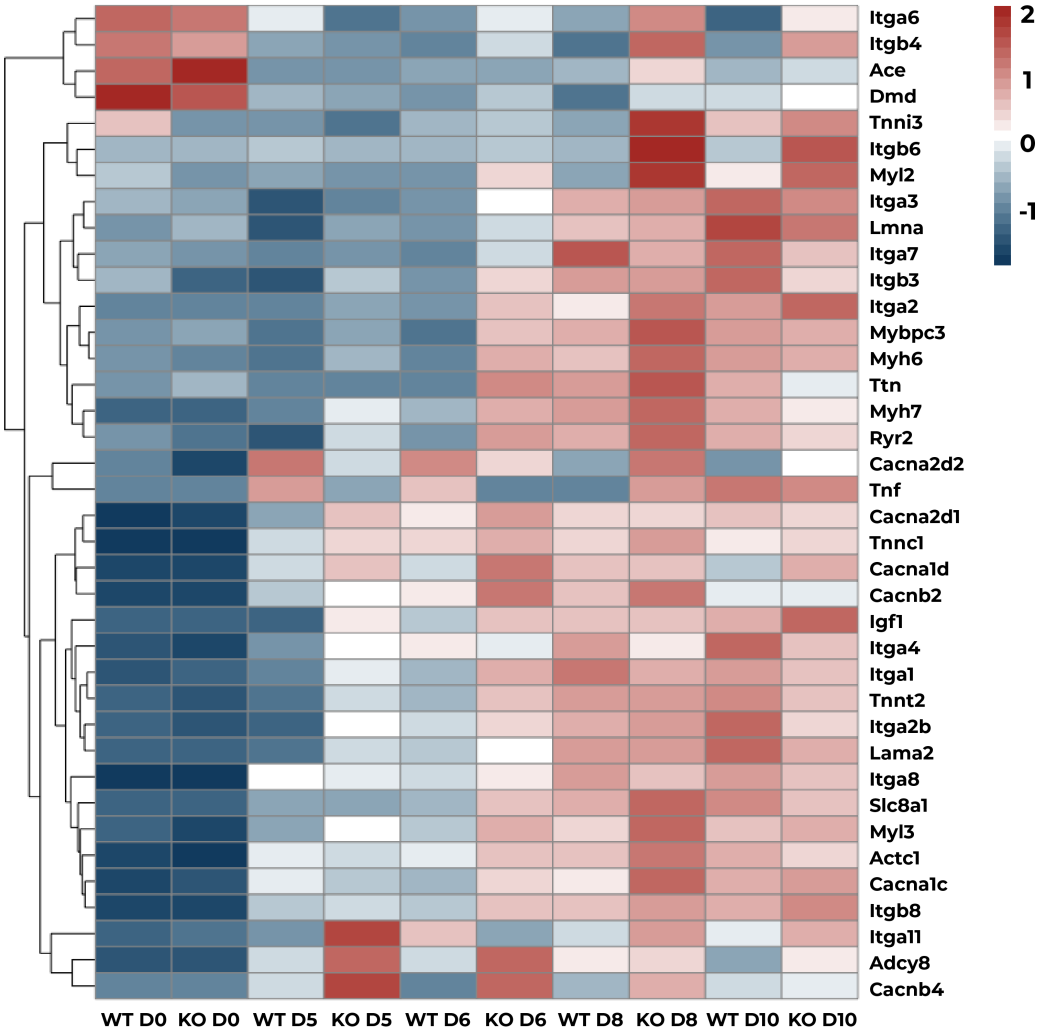

Figure 4.8 – Heat map of differentially genes that overlap with "Hypertrophic cardiomyopathy" and "Dilated cardiomyopathy" GO terms. Profiles of expression were hierarchically clustered. Colors correspond to Z-score.

On Figure 4.9 we can see CPM values for different genes, grouped by the type of proteins they encode. The first group of genes encodes proteins that will be part of the contractile unit of CMs, *Myh6*, *Myh7* and *Myl3* (Figure 4.9 A). These genes start to be upregulated early on KO samples, even before EB platting. In our dataset, the expression of these genes in KO samples seems to peak at day 8 of EB differentiation, showing lower levels of expression at day 10. By comparison, WT samples do not express these genes as strongly as KO samples, at least in the days analysed. For two genes, *Myh6* and *Myh7*, at day 10 WT samples show higher CPM levels. Next, we probed the expression of genes encoding calcium channel subunits, *Cacna1d*, *Cacna2d2*, and *Cacna1c* (Figure 4.9 B). These three genes encode proteins that will form L type calcium channels, typical of cardiomyocytes. For *Cacna1d* we see an early upregulation in KO samples, while for *Cacna1c* that upregulation only occurs later. As for the *Cacna2d2*, the opposite pattern can be observed, with early expression in WT samples, that decreases with time, while KO samples increase their *Cacna2d2* expression until its peak at day 8. The last group of genes that we analysed corresponds to genes encoding integrin subunits, namely the subunits most associated with cardiomyocytes: *Itga1*, *Itga3*, and *Itga7* (Figure 4.9 C). These three genes are expressed differently, as can be noted from their range of CPM values. *Itga1* is upregulated first on KO samples, and its expression is higher for KO samples at days 5 and 6. For days 8 and 10, however, the pattern is reversed, and WT samples express more *Itga1*. Overall expression levels of *Itga3* are the

highest on our data set, and differences between WT and KO samples are more noticeable at days 6 and 10. For the other timepoints in our dataset, levels of *Itga3* expression are similar between the two EB types, with higher expression on KO samples at days 6 and 8. *Itga7* expression is low, maximum of ~10 CPMs on WT D8. This gene is upregulated first on KO samples, but on the D8 WT sample, its expression surpasses the KO expression. Finally, expression levels of *Itga3*, although at high CPM levels, do not follow a trend. On days 0 and 10, WT samples express more *Itga3*, but on days 5, 6 and 8, KO EBs are the ones expressing

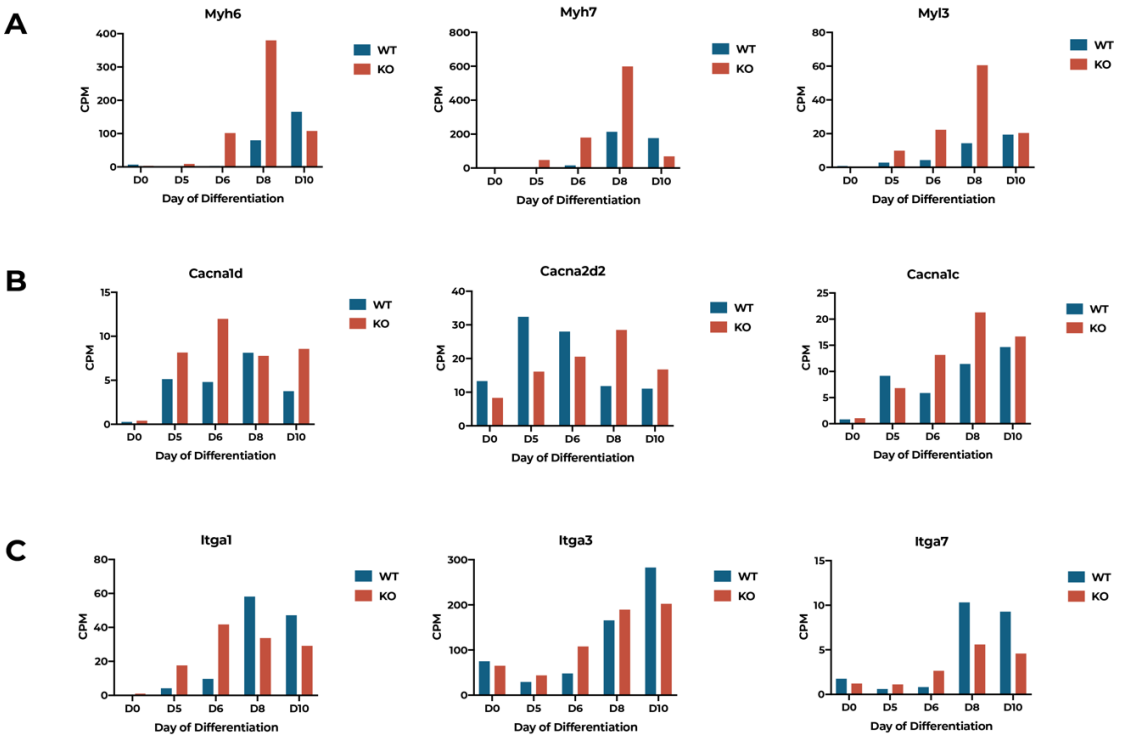

Figure 4.9 - Counts per million of different genes related with cardiac differentiation; A) genes encoding sarcomere components; B) genes encoding subunits of calcium channels; C) genes encoding integrin subunits

more *Itga3*.

4.2.4 Dand5 influences genetic expression associated with Notch and Wnt signalling pathways

Following the ORA results pointing towards a possible influence of DAND5 in several signalling pathways, two specific pathways were investigated, Wnt and Notch, the only two pathways that are strongly involved in cardiac development and were significantly altered in our ORA analysis. Figure 4.10 A shows a heatmap with DEGs overlapping with the Notch GO term. There we can see that, when no *Dand5* is expressed during EB differentiation, genetic expression of Notch signalling components is altered. At day 0, the main differences are observed in the genes *Dtx3l* and *Dll1*, with other genes presenting similar levels of expression. After that time point, the overall pattern shows lower expression levels in KO samples.

To better understand the heat map, we decided to plot CPM levels for different genes encoding Notch signalling players. *Dll3*, *Dll1* and *Jag1* encode Notch activating ligands, while *Notch1* encodes the membrane receptor of the pathway. *Rbpj* encodes the transcriptional regulator in charge of transducing intercellularly the signal. Finally, *Hes1* is one of Notch's target genes, that is upregulated upon activation of the pathway. Figure 4.10 B shows that two of the ligands, *Dll1* and *Dll3*, are more expressed on WT samples, up to day 8. As for the third ligand, *Jag1*, its CPM values are higher on WT samples on day 5, higher

on KO samples at later stages, and display similar values at days 0 and 6. On the other hand, *Notch1* genetic expression does not show stark differences, except at day 5 of EB differentiation, when KO levels are lower. The expression of *Rbpj* shows that, after day 0, there is a great reduction in expression and WT samples display higher CPM levels. Lastly, WT samples show higher expression of *Hes1*

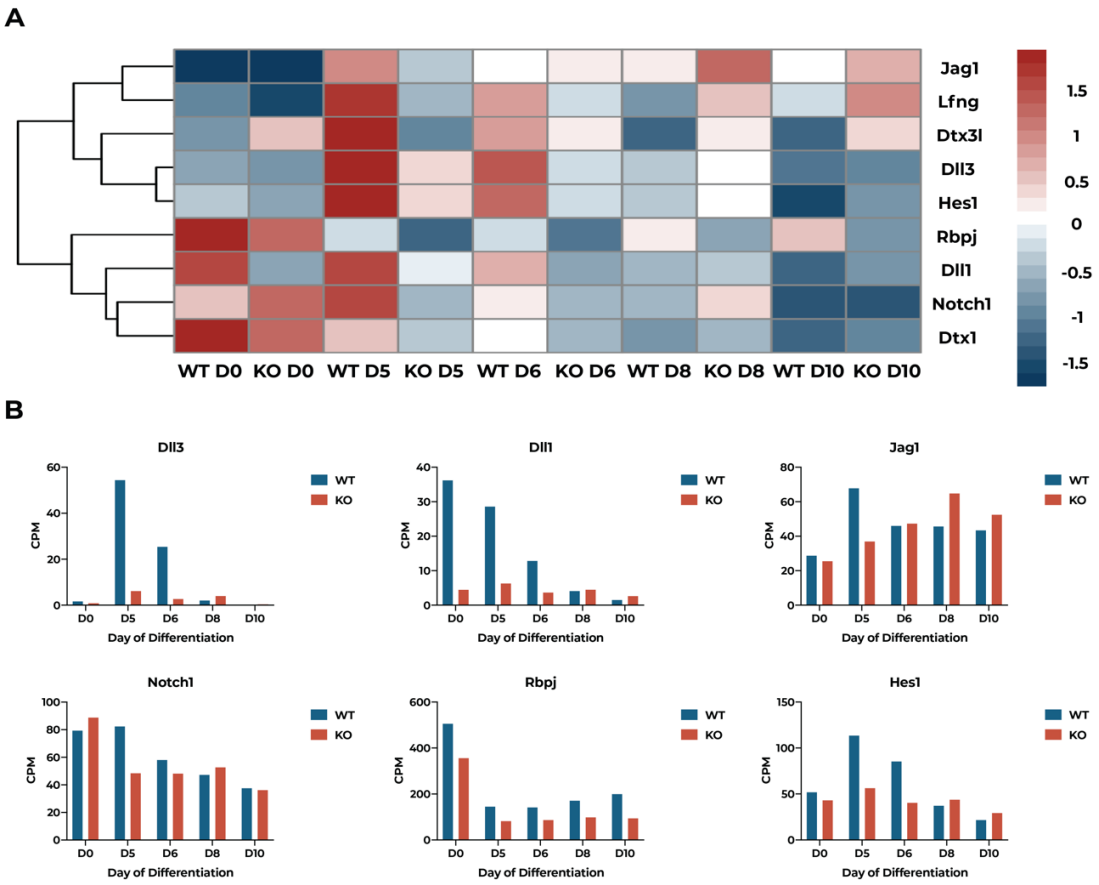

Figure 4.10 - Genetic expression changes in *Dand5* KO; A) Heat map of genes encoding Notch signalling pathway. Profiles of expression were hierarchically clustered. Colours correspond to Z-score; B) Counts per million of genes encoding proteins involved in Notch signalling.

until day 8, when the pattern is reversed, and KO samples start displaying slightly higher CPM levels for this gene.

The heat map for the genes overlapping with GO term Wnt pathway can be seen on Figure 4.11 A. The first group of genes at the top, including *Wnt3a* and *Fzd10*, ligand and receptor, respectively, is upregulated early only in WT samples, but its expression decreases over time. A middle cluster of genetic expression that includes genes such as *Wnt4* and *Nkd2*, encoding a ligand and a negative regulator, respectively, displays a more heterogenous pattern, with most genes being lowly expressed at the initial time points of the data set. As differentiation progresses, this cluster of genes seems to be upregulated, but again the pattern is very heterogeneous and does not allow to establish an obvious comparison between WT and KO samples. Figure 4.11 B, shows the CPM values for several genes involved in the Wnt pathway. *Axin2*, a gene that encodes a scaffold protein important for transducing canonical Wnt, and *Tcf7*, that encodes a transcription factor that carries out Wnt signals on the nucleus, are more expressed in WT samples for days 5 and 6, with days 8 and 10 showing similar CPM values for these genes. *Lef1*, that encodes a TF that regulates genetic expression downstream of Wnt, and *Ccnd1*, one of the target genes of Wnt that influences

the progression of the cell cycle, share similar patterns of expression. Initially, KO cells display a higher number of these transcripts. At days 5 and 6 of EB differentiation, these two genes are more expressed on WT samples. The overall

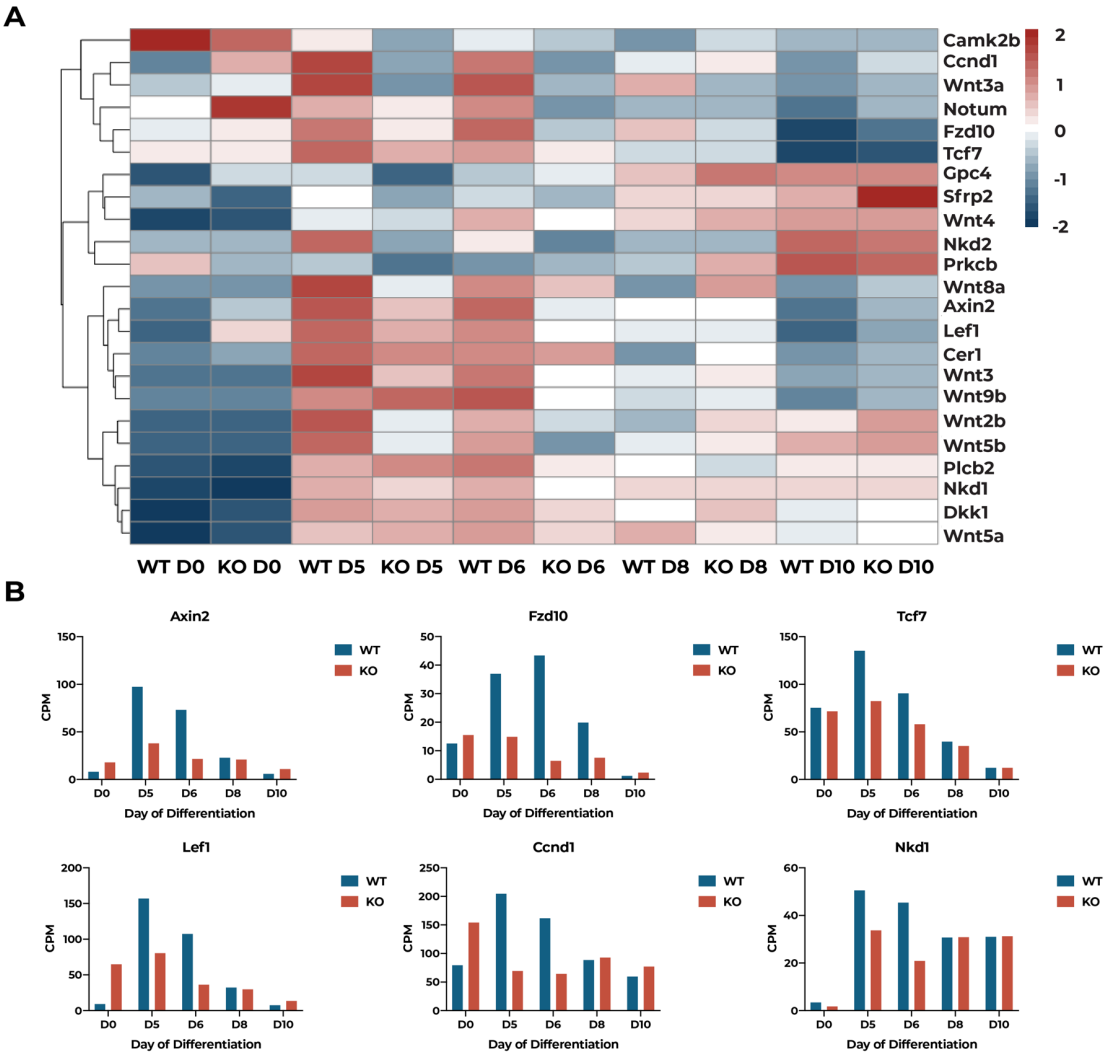

Figure 4.11 - Genetic expression changes in *Dand5* KO; A) Heat map of genes encoding Wnt signalling pathway. Profiles of expression were hierarchically clustered. Colours correspond to Z-score; B) Counts per million of genes encoding proteins involved in Wnt signalling.

expression of these genes decreases for samples of days 8 and 10, and its CPM levels are similar in both EB types. *Fzd10* encodes a membrane receptor that

allows individual activation of all Wnt pathways. Even though the expression of this gene is only slightly higher in KO samples at day 0, on days 5, 6, and 8, with both EB types expressing low levels of *Fzd10* at day 10. Lastly, *Nkd1*, encoding an intercellular modulator that inhibits canonical Wnt while upregulating planar cell polarity Wnt pathway, shows negligible CPM values for day 0, and is more expressed in WT samples than KO on days 5 and 6. This gene is similarly expressed on both cell types on days 8 and 10 of EB differentiation.

The CPM values depicted on Figure 4.11 B do not show any gene encoding a Wnt ligand. Due to their specific role and diversity, the CPM values of Wnt ligand-encoding genes that appeared on the ORA are shown on Figure 4.12. Even though CPMs display different ranges, there seems to be a common expression pattern for *Wnt5b, Wnt3*, *Wnt8a*, and *Wnt2b*, with almost no expression at day 0,

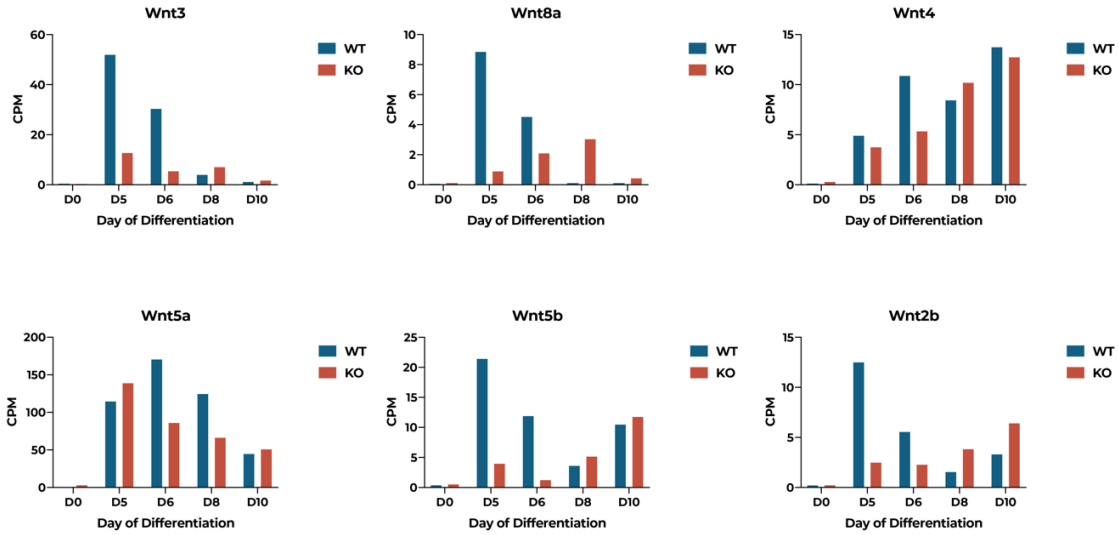

Figure 4.12 -Counts per million of DEGs encoding Wnt ligands.

higher expression on WT samples for days 5 and 6, and then higher expression on KO EBs for days 8 and 10. *Wnt4* and *Wnt5a* display a different expression pattern when compared with other Wnt ligands. WT EBs expressing more *Wnt4* in every time point, except for day 8, when KO cells display slightly higher CPM values. As for *Wnt5a*, after low expression on day 0, at day 5 KO cells show higher CPM values, while at days 6 and 8 WT EBs were found to have more *Wnt5a* transcripts then their KO counterparts. On day 10 of differentiation, *Wnt5a* levels show an overall decrease, and similar expression levels on both EB types.

4.3 Discussion

In this chapter, we have probed the genetic expression changes in EB differentiation in *Dand5* KO cells. Initial analysis showed that the depletion of *Dand5* leads to a temporal shift in EB differentiation, causing EBs to progress faster through differentiation. The BMP and Wnt antagonist role of *Dand5*[89] might partially explain this. In development, BMP and Wnt signalling pathways are in charge of embryo patterning before gastrulation[111,112], and will be responsible for the development of several organs. As such, it is only expected that when an antagonist is depleted, EB differentiation will be different, since temporal differences in patterning will lead to differences in cell differentiation and EB development.

Individual ORA analyses for each day allowed us to overview the differences between both cell lines. Regarding MF, DEGs mostly encode genes that will affect TF binding to DNA, cell adhesion molecule binding, and ECM constituents. Differences in the activation of signalling pathways will lead to differences in genetic expression, hence altering TFs binding to DNA, and influencing gene expression. Following the same rationale, WT and KO EBs will follow different differentiation paths, with cells secreting distinct ECM proteins and producing different membrane proteins and adhesion molecules. In agreement with the MF results, we mostly see BP terms related with regulation of cell differentiation, namely neuronal and cardiac differentiation. The terms pertaining to neuronal differentiation agree with Pathway ORA results, that also show downregulation of genes overlapping with GO term “Axon guidance”. Wnt dysregulation might be behind such results, since Wnt inhibition results in neural induction[109], while its activation patterns EBs for PS-like differentiation[109]. The results for CC ORA indicate that the DEGs encode proteins located to the membrane or to the extracellular space. ORA MF, BP, and CC results suggest that *Dand5* KO EBs differences from their WT counterparts reside mainly in membrane proteins, ECM secretion, and TF activity. As all these factors influence each other, it is hard to discern a specific role for DAND5 in EB differentiation from these results.

The Pathway ORA results enabled the assessment of which cell pathways are affected by the depletion of *Dand5*. As differentiation progresses,

downregulated terms include signalling pathways such as Notch, Hippo, Wnt, or MAPK. The upregulated terms are related with cardiac differentiation, cell adhesion molecules, or focal adhesion. These results are in line with the results from the other types of ORA, and further confirm the notion that KO EB cells, upon exiting pluripotency, will differentiate into different cell types than their WT counterparts.

Further probing into the DEGs overlapping with GO terms related with cardiac differentiation or cardiomyocyte differentiation showed earlier expression of genes encoding cardiac sarcomere proteins and calcium channels in KO samples. This is in line with our previous report *in vivo*, that detail how *Dand5* KO mice have thickened myocardial walls[97], and *in vitro*, where we report the enhancement of cardiac features in KO EBs. The anticipated upregulation of cardiac-related genes is the basis for the earlier emergence of beating foci in KO EBs, at around days 6 and 7 of differentiation.

We have reported that this temporal difference is based on an earlier mesoderm induction in *Dand5* KO EBs[99]. Mesoderm induction *in vivo* depends on epiblast cells undergoing EMT and subsequently ingress through the PS[4,113]. The *in vitro* report[99] showed that DAND5 expression starts at day 2 and peaks at day 4 of differentiation on WT EBs. We also showed that KO EBs display an anticipated peak in *Mesp1* expression, at day 3[99]. These results indicate that, when no DAND5 is expressed, *Mesp1* is upregulated earlier. A report by Ueno

and colleagues found that, in EBs, treatment with WNT3A leads to anticipated *Mesp1* expression. Given the reported inhibition of this molecule by DAND5[91], *Mesp1* induction could occur earlier due to accumulation of WNT3A, leading to anticipated mesoderm induction[3,109].

There is a myriad of signalling pathways influencing PS and Mesoderm induction, but Wnt, BMP and FGF pathways assume particularly important roles[3,12,33]. As seen in the pathway ORA results, Wnt is dysregulated in KO samples on the days analysed. Assessing expression of specific Wnt pathway elements, we see that WT cells seem to be activating both canonical and non-canonical Wnt, namely by the CPM values of canonical (e.g., *Wnt3*) and non-canonical Wnt ligands (e.g., *Wnt5b*), both canonical and non-canonical (*Wnt5a* and *Wnt5b*). Bearing in mind that DAND5 has been described as inhibiting some elements of the Wnt pathway[91], the reverse result would be expected, persistent upregulation of Wnt pathway, and delayed emergence of cardiac features. However, signalling and EB dynamics must be considered. During embryonic development, Wnt pathways show precise patterns of activation, and, in the case of cardiac differentiation, there is a sequential activation of canonical and non-canonical pathways[114]. The same tight regulation has been shown to be required in mESC differentiation into cardiomyocytes[115]. This would make it so that KO EBs, on the days analysed, have already activated Wnt signalling, explaining the downregulation of this term in the Pathway ORA results seen on Figure 4.4 and

Figure 4.5. A more detailed study of days 1 through 4 of EB differentiation should be done to evaluate Wnt activation before the development of cardiac features in KO EBs. Besides Wnt, it would be expected that KO EBs upregulated TGF-β signalling, more specifically, BMP and Nodal pathways. We do not see this in our ORA results, which can be explained by different regulatory mechanisms being activated to maintain signalling levels, such as expression of *Lefty1* or *Lefty2*[116,117]. The redundancy of BMP and Nodal pathways has been previously reported[118,119], and the non-lethal DAND5 KO mice also point towards a considerable level of redundancy of DAND5 target pathways.

The RNAseq analysis showed that, besides Wnt, there are other pathways that are differentially regulated in WT and KO EBs. Given its role in development[120] and in cell transformation[121,122], we decided to probe deeper into Notch signalling pathway. While for Wnt we saw a temporal shift, in Notch it seems that depletion of *Dand5* leads to lower expression of its components, denoting what might be lower activation of this pathway. Even though EMT is regulated by several pathways, with an equal diversity of cell state outcomes[65], TGF-β, Wnt, and Notch play an important role in its induction. Taking this into account, distinct patterns of activation for those pathways will lead to different degrees of EMT and respective cell state outcomes.

The depletion of *Dand5* causes a differential activation of pathway such as Wnt or Notch. Coupled with earlier expression of Brachyury in KO EBs[99], the cell

differentiation path will be altered, promoting cardiac lineages. It will also influence the expression of genes associated with how cells interact with their microenvironment, and what kind of ECM they will produce. Genetic expression studies are not an endpoint, requiring further studies to prove that differences in transcription are effectively differences in protein synthesis.

Chapter 5 – Loss of DAND5 disrupts EMT *in vitro* and leads to valve defects *in vivo*

5.1 Introduction

The results from Chapter 4 indicate that *Dand5* KO EBs differentially express key genes associated with stem cell differentiation. Most notably, KO EBs display an anticipation of mesoderm induction and cardiac differentiation. The enhancement of cardiac features in *Dand5* KO EBs was already detailed and reported elsewhere[99]. This difference in cell potential might result from the disruption of signalling pathways, namely Wnt, reported on the previous chapter. This pathway is directed involved in directing cells towards cardiac fates[34,123], while also influencing further cell maturation. Furthermore, together with Notch, these pathways will not only directly influence gene expression, but they will rather target both genetic and cellular features, with Wnt and Notch pathways being associated with EMT[123–125]. All in all, the effect of these pathways on cell differentiation is due to changes in both genetic expression and cell state. Bearing in mind the possible differences in cell states in KO EBs, in this chapter we analyse distinct EB features associated with EMT, namely migration, attachment to the substrate and expression of EMT genes. While the expression of EMT

genes is anticipated in KO samples, the migration behaviour and the interaction with the substrate seem to reflect a more epithelial phenotype.

Furthermore, taking into account the possible role in EMT and the proven role in heart development[97], we hypothesize that the effects of *Dand5* in mouse development might be wider than myocardium organisation and maturation. More specifically, DAND5 could play a role in the cardiac developmental EMT/EndMT. In this chapter, we will also report this potential *in vivo* role in valve development using *Dand5* KO mice and probing into heart valves as an *in vivo* model for EMT. Our results show the expression of *Dand5* at valve sites, and some KO mice harbour valve morphological defects.

5.2 Results

5.2.1 *Dand5* KO EBs spread less upon plating and establish more focal contacts with the substrate

In some EBs differentiation methods, it has been reported that the moment at which they are platted induces EMT and subsequent mesoderm differentiation. In our experiments, *Dand5* KO EBs display morphological and spreading differences upon platting, which lead us to investigate whether these are significant when compared with WT EBs.

This spreading movement was closely monitored up to 36 h after plating at day 5, measuring spreading areas every 12 h. While WT EBs show significant spread and morphological change, KO EBs cover smaller areas over time, while slowly changing their morphology (Figure 5.1 A). Upon quantification of the areas covered by EBs, the initial visual observations were confirmed (Figure 5.1 B). At 24 h after plating, the relative spreading areas show a small difference, while at the final time point (36 h) these changes are starker, with KO EBs displaying a smaller relative spreading area.

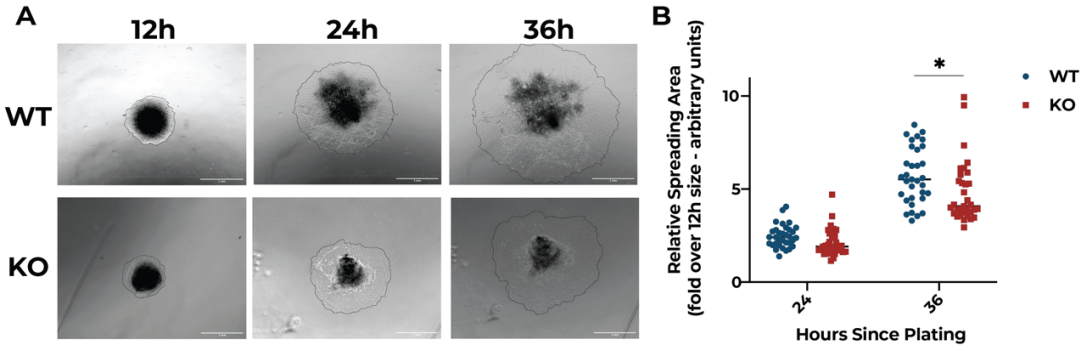

Figure 5.1 – A) Brightfield imaging pictures of EBs at 12, 24 and 36 hours after plating onto gelatine-coated wells. Scale bars – 1 mm; B) Relative spreading area of EBs at 24 and 36 hours after plating. Individual points represent individual values for the ratio with measured size at 12 hours after plating, for independent EBs (n=33). At 36 hours, multiple t-tests statistical testing revealed statistical significance, with a p-value of 0.0242.

In order to further understand these differences in spreading, we proceeded to assess how cells on the spreading border interacted with the gelatine ECM of the culture wells. One of the most common ways that cells use to attach and to migrate on a substrate is through focal protein complexes, namely FAs. To evaluate how EBs organise FAs, we fixed and stained EBs at days 6 and 7 of

differentiation for vinculin, a protein that integrates FA complexes. On Figure 5.2 A, a higher number of focal adhesions on the KO cells can be seen. Upon quantification of these adhesion points (Figure 5.2 B), we observed that KO samples presented both a higher number as well as larger FAs, with significant differences in area covered by FAs at day 6.

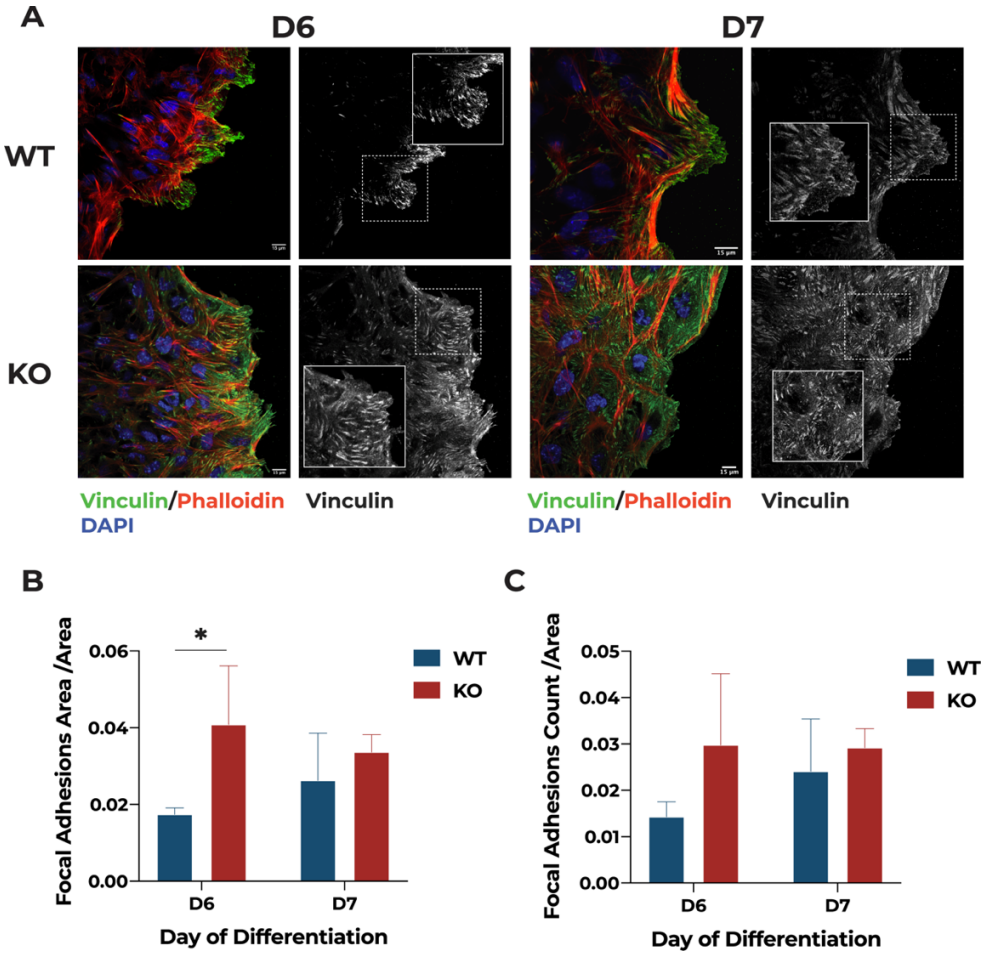

Figure 5.2 – A) Fluorescence images of EBs at days 6 and 7, stained for phalloidin (red), vinculin (green) and DAPI (blue). Vinculin channel shown separately in greyscale, with augmented boxed areas. Scale bars - 15 μm; B) Quantification of focal adhesions' area at days 6 ($p = 0.022$) and 7, normalised with area covered by cells. Bars represent mean with SD (n=3); C) Quantification of focal adhesions number at days 6 and 7, normalised with area covered by cells. Bars represent mean with SD (n=3).

5.2.2 KO EB cells migrate less in wound healing assays

Cell signalling and differentiation are not homogenous across EBs, nor are the several stimuli that cells respond to. As such, we hypothesized that the differences in spreading detailed in section 5.2.1 might result from different cells at the surface of EBs, with cells on the inner part being similar, or from higher levels of FAs.

To address this question and assess whether there was a difference between inner and outer cells, we performed a wound healing assay using cells from dissociated EBs. At day 5, EBs were dissociated, and cells were plated in gelatine-coated wells. Upon reaching confluency, cells were mitotically inactivated with Mitomycin C, and a scratch (wound) was done in the cell monolayer. We monitored the evolution of this wound in both cell lines for 8 h, time at which most of the WT cells had completely closed the wound (Figure 5.3 A).

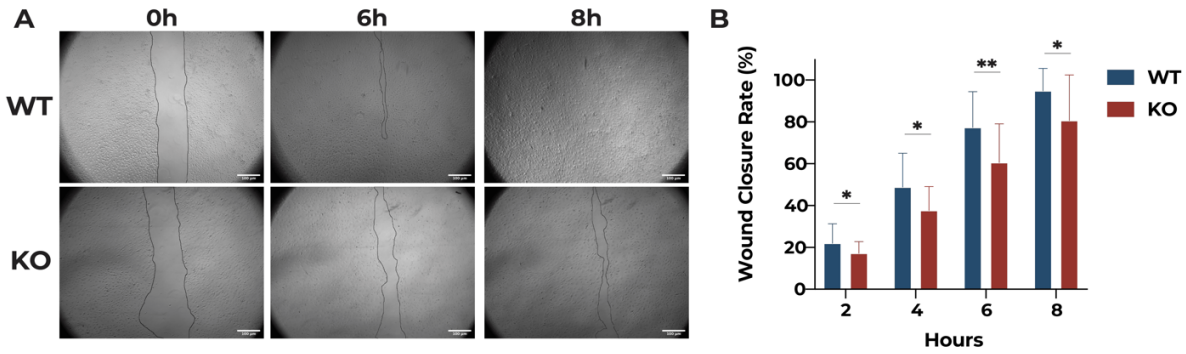

Figure 5.3 - A) Brightfield images picturing wound areas at the beginning of the wound closure assay (0 hours) and correspondent images at 6 and 8 hours after. Scale bars - 100 µm; B) Quantification of wound closure rate by ratio with scratch at 0 hours (n=32), with bars depicting mean and SD. Statistical significance was analysed with multiple t-tests. Significant results were found at 2 hours (p=0.0143), 4 hours (p=0.0046), 6 hours (p=0.0015) and 8 hours (p=0.0046).

Indeed, further quantification of these images showed that KO cells did migrate slower (Figure 5.3 B). This shows that, rather than a difference at the outermost cells of EBs, the depletion of DAND5 leads to a general change in differentiation and/or ability to establish contacts with the substract.

5.2.3 The expression of key EMT TFs and membrane proteins is disrupted in *Dand5* KO EBs

The differences in EB spreading, FA content, and cell migratory behaviours led us to consider that, during differentiation, EMT might be affected. EBs undergo an EMT-like process to induce mesoderm differentiation, and it is this process that allows clonal-like mESCs to differentiate and migrate. To do so, we decided to check the expression of transcription factors responsible for EMT, such as *Snai1*, *Snai2*, *Prickle,* and *Twist1* (Figure 5.4). By real time quantitative PCR (RT-qPCR), we analysed the relative expression of these markers and observed that there seems to be a temporal shift in the KO samples, except for *Prickle*. When no

DAND5 is produced, cells seem to go faster through differentiation, expressing EMT transcription factors sooner than the WT counterparts.

Another aspect that we assessed was the expression of membrane markers *Cdh1*, *Cdh2*, and *EpCAM*. CDH1 and EPCAM are key membrane proteins of epithelial cells, while CDH2 is a prototypical cadherin of the mesenchymal profile. The results on Figure 5.5 show that *Cdh1* expression decreases along KO differentiation, with a difference from the WT pattern at day 4, where lower levels

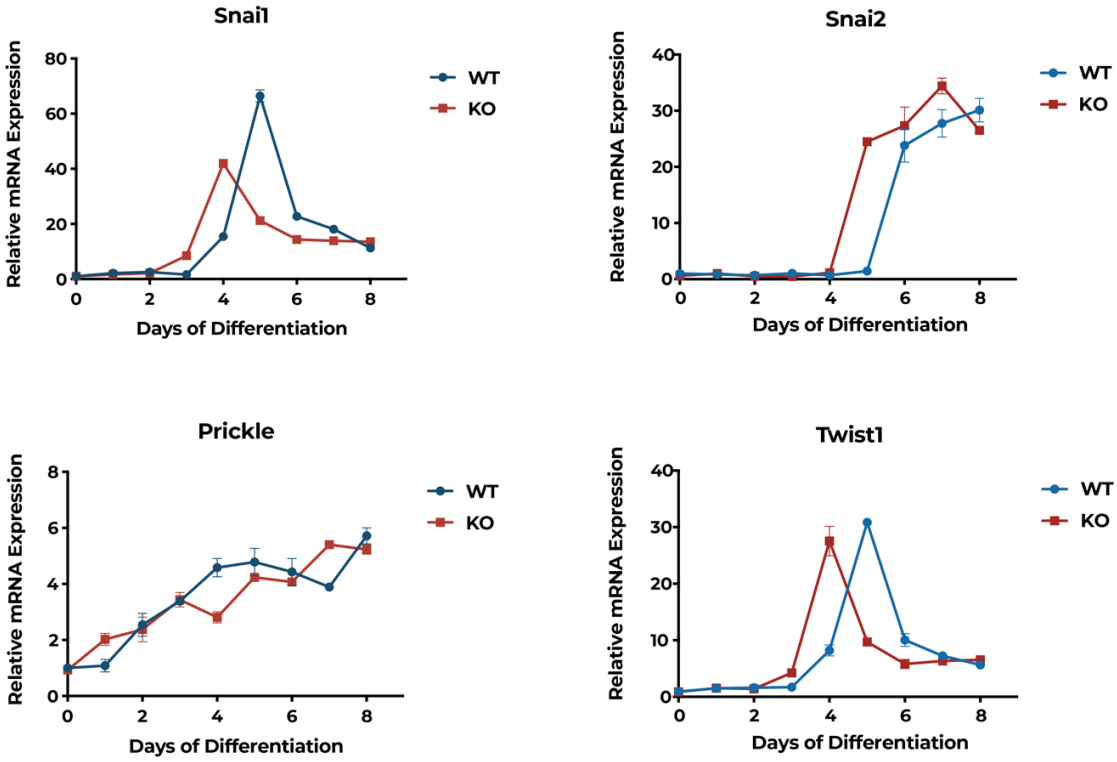

Figure 5.4 – Genetic expression of key epithelial to mesenchymal transcription factors, *Snai1*, *Snai2*, *Prickle*, and *Twist1*. Results represent representative mean with SD of three different technical replicates.

can be observed on KO cells. For the other epithelial marker, *EpCAM*, we see that the KO cells up regulate its expression earlier than the WT, and they also

repress it earlier. This temporal shift can also be observed in the expression profile of *Cdh2*, but at later days of EB differentiation.

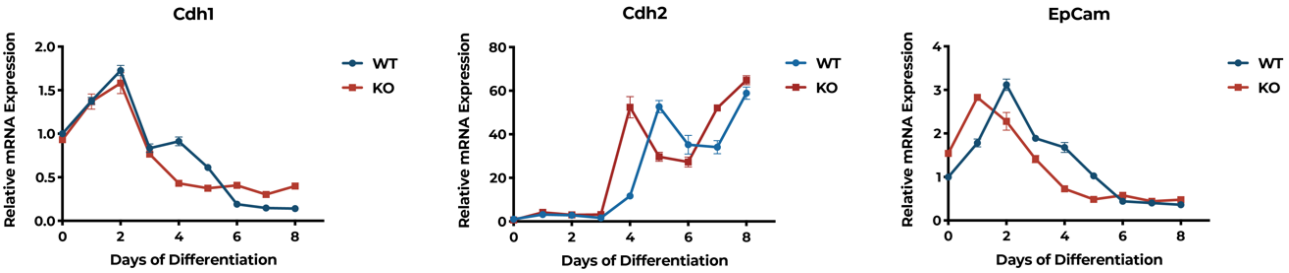

Figure 5.5 - Genetic expression of key epithelial and mesenchymal membrane markers, *Cdh1*, *Cdh2*, and *EpCAM*. Results represent representative mean with SD of three different technical replicates.

5.2.4 *Dand5* KO mouse shows EndMT defects during cardiac valve development

Apart from the previously observed stronger induction of cardiac features[99], our EBs harbour EMT defects that seem to influence migration. If these differences are meaningful within the *in vivo* context, it will lead to defects in development. Given the results of RNAseq and RT-qPCR, that indicated

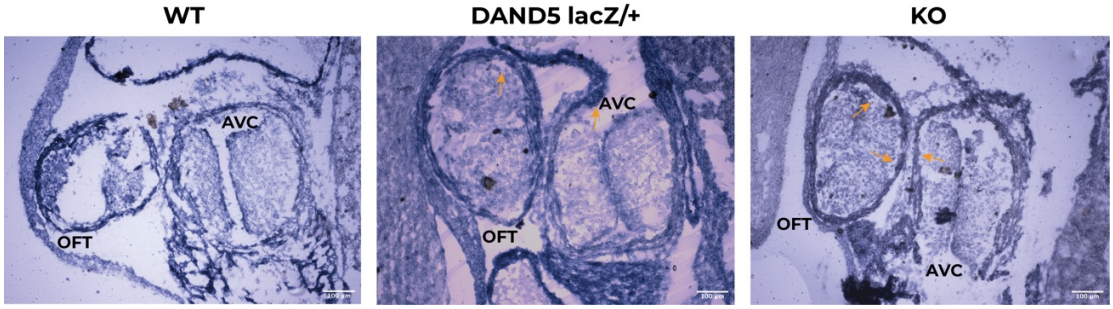

Figure 5.6 - lacZ staining of WT, DAND5 lacZ/+, and KO embryos at E11.5, showing developing valves. Orange rows indicate locations with significant lacZ staining. Scale bars - 100 µm.

alterations in Bmp, Notch, and Wnt activation, those *in vivo* effects may influence the EndMT process required for correct formation of heart valves.

Using our mouse *Dand5*-KO model, we obtained heterozygous foetuses (*Dand5* lacZ/+) at E11.5, time at which EndMT is occurring in heart valves, allowing us to check whether *Dand5* is being expressed at this time of development and the localization of such expression. Comparing Salmon-Gal lacZ staining in WT, DAND5 lacZ/+, and KO embryos (Figure 5.6), we observe that *Dand5* expression is being activated at this time of development, and that is localized to the myocardium that underlies the OFT and AVC valve.

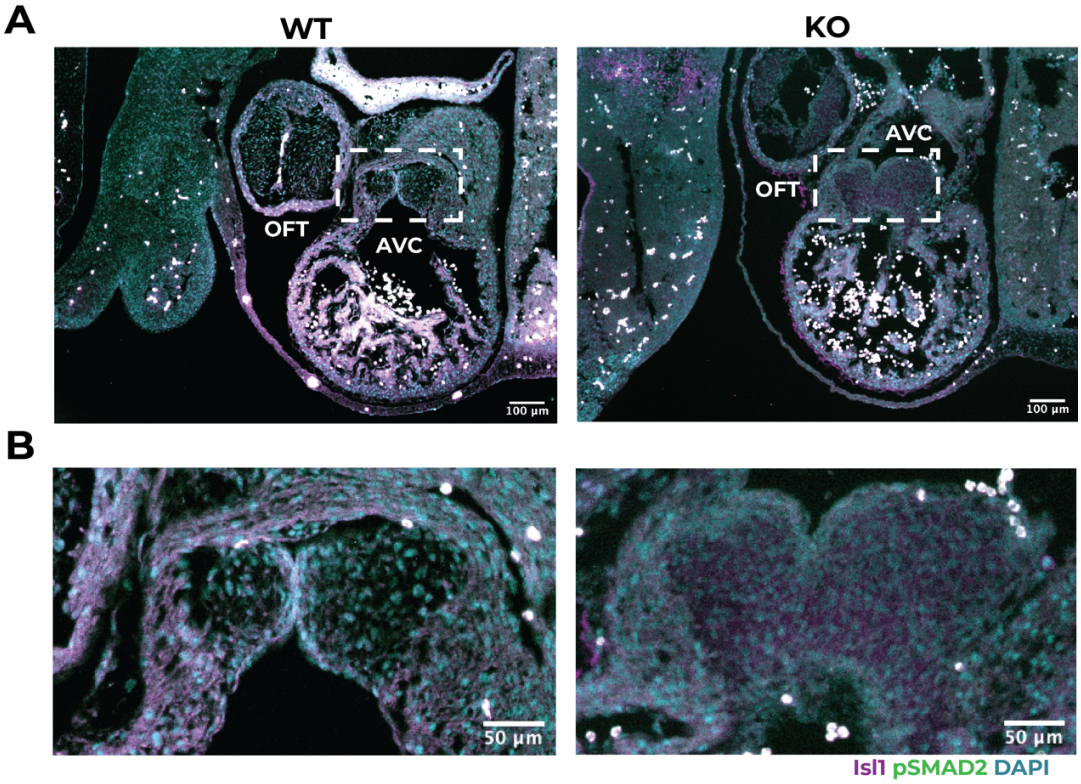

Figure 5.7 – A) Isl1, pSMAD2 and DAPI staining of WT and KO embryos at E11.5, showing developing valves. Scale bars - 100 µm; B) Amplification of boxed regions. Scale bars - 50 µm.

In some KO embryos, we noticed that heart valves displayed altered morphologies, namely inversion of the leaflets. We proceeded to perform immunostaining for ISL1, to identify SHF-derived cells, and pSMAD2, to assess signalling alterations within the valves. This staining showed morphological defects on KO heart valves (Figure 5.7), that display inversion of the leaflets. Even though we could not observe differences in pSMAD2 staining, we observed that developing valves do not seem to have the same structure. KO valves appear to be inverted, when compared with WT ones. Moreover, cellular differences can also be observed, with KO valves appearing enlarged and more disorganised than their WT counterparts.

5.3 Discussion

The exploration of RNAseq data from KO and WT EB differentiation showed that *Dand5* depletion influences the expression of signalling pathways that are highly important for mESC differentiation, while simultaneously influencing EMT. We also saw quite distinct morphologies that lead us to investigate whether EMT was altered in EBs. The results in this chapter show that KO EBs do undergo EMT at a different pace, at least. Their lower spreading areas indicate that cells are either not poised to migrate as much as the WT, or they cannot spread away from the centre of the EB. This can be a result of a more epithelial phenotype, or a

cellular obstacle to turn over attachment clusters. Upon migration, FAs need to be disassembled and assembled again at a different cell membrane location, if cells are to migrate[126–128]. Stronger vinculin contents, and hence more FAs, show that the depletion of DAND5 during EB differentiation possibly overstimulates FA formation or limits its turnover. The turnover of FAs is a complex process that involves different molecules, such as Focal Adhesion Kinase or Src Kinases, that in turn are regulated by different signalling pathways[129–131].

BMP is one of the pathways involved in regulating cellular attachment and interaction with the microenvironment, with recent reports relating that different BMP players elicit different biomechanical responses[132]. Among all the different BMP molecules, BMP4 displayed strong influence on adhesion and cell spreading[132]. On the other hand, this molecule has been reported to induce EMT and mesoderm differentiation in hESCs[133]. Given that DAND5 has been reported to antagonize BMP4[89], our results on anticipated mesodermal differentiation would be explained by lower inhibition of BMP4. BMP2 is another protein that has also been associated with initiating and coordinating EMT *in vivo*[134] and is differentially expressed in KO EBs[99]. However, the results on EMT disruption do not follow this pattern, since cells spread and migrate less. This difference could be explained by alterations in BMP2 signalling partner, the Notch pathway[134,135], that would hinder the full EMT extent.

One of the aspects that could be interfering with cell attachment and spreading is the type and organisation of membrane proteins. Most notably, the expression of specific integrin subunits is associated with modulation of specific pathways and cellular states[127,130,136]. Going back to Figure 4.8 on section 4.2.3, a difference in expression of distinct integrins can be observed. Most notably, the expression of *Itgb3*, which has been associated with increased cell adhesion[132,137], is higher in KO samples on days 5 and 6 of differentiation. Further experiments that assess ITGB3 levels in WT and KO EBs are necessary to understand whether this molecule might be behind the defects in migration. Pharmacological inhibition of the differentially expressed integrin subunits could also be studied for rescue experiments using KO EBs.

The nature, timing, and number of contacts that *Dand5* KO cells establish with their environment will further influence how cells transform. If cells are not able to break down AJs, for example, β-catenin will not be released, hindering EMT, since there will be lower rates of β-catenin-dependent signal transduction[124,138]. The interplay between cell contacts turnover and signalling influences genetic expression significantly. Following the differences in migration and FA proteins, our cells display different patterns of expression of key EMT TFs and membrane proteins, such as *Snai1* and *Cdh1*. Expression of TFs is anticipated in KO cells, and the expression of membrane markers seems to indicate that those cells acquire a mesenchymal profile earlier. Induction of EMT

TFs expression might result from the earlier Wnt activation, that also contributes towards anticipation of cardiac features[33,124], or to direct upregulation by MESP1, which has been shown to directly upregulate *Snai1* and *Twist1*[27]. The expected outcome from anticipating EMT TFs expression would be more cell motility, which does not seem to be the case. The differences observed later in EB differentiation could result from post-transcriptional regulation of EMT TFs, or to regulatory signalling loops that will lead to differences in the cellular state.

These results should be used as a steppingstone for experiments that assess protein levels and location, namely of EMT TFs and membrane markers. By assessing the location of CDH1 or β-catenin, which are part of AJ and, upon breakage, transduce EMT signalling[78,124], it could be possible to understand the kind of contacts cells are establishing, and whether the signal is being correctly carried out. Platting EBs in substrates with different mechanical properties should also be done, since cells react differently to variations in ECM stiffness[132,139], and mESC differentiation can be influenced by mechanical cues[140]. Experimenting with substrate stiffness could help understand whether DAND5 is involved in sensing extrinsical mechanical cues. These signals are sensed and carried through defined pathways. For example, BMP2 has been shown to cooperate with the mechanotransducive YAP/TAZ pathway in osteogenesis differentiation[141]. The authors showed that the latter is required to promote BMP2-driven osteogenesis, since it induces the expression of YAP/TAZ TFs. Given that the

depletion of DAND5 induces significant changes of membrane proteins, including signalling receptors, it could be involved in a mechanotransduction or mechanosensing pathway. If true, substrates with distinct stiffness would elicit different cellular responses.

Besides the *in vitro* results, we looked into our *in vivo* model for signs of EMT disruption. In this chapter we report a new location of *Dand5* expression during mouse development, on myocardial cells at OFT and AVC sites. Furthermore, we show that this expression has an influence in the morphological development of those sites, with some of the KO mice displaying heart valves morphological defects. This phenotype is in line with the studies that detail the influence of myocardial signalling in valve development[142,143].. This cellular layer is the responsible for patterning BMP signalling during EndMT[81], initiating and controlling valve differentiation in a paracrine way.

Our results are only phenotypical, and further studies are required to understand how does DAND5 influence EndMT, valve sites patterning and organisation, cell and ECM content, and valve function. Given its extracellular antagonist function, in valve development DAND5 might be responsible for fine tuning BMP patterning, ensuring proper expression of valve development genes, or it could be important for EndMT regulation at those sites[134,135]. This second hypothesis seems more likely if we consider the results of Chapter 4 . Following those *in vitro* results, and considering a developmental context, it seems as if

DAND5 KO cells are unable to organise themselves properly. Hence, the resulting compromising of heart valve structure. Further studies should be performed to clarify the role of DAND5 in valve development. KO valve cushion explants could be used to understand whether there are differences in EndMT, or if the altered phenotype is just a downstream result from the role of DAND5 in heart development.

Chapter 6 - General discussion and future perspectives

In this work, we have provided evidence suggesting that DAND5 range of action goes beyond LR asymmetry establishment during early development. Monitoring the genetic expression of both WT and *Dand5* KO differentiating mESCs revealed different genetic expression patterns. These changes in expression of key developmental signalling pathways activate distinct pathways upon exiting pluripotency, leading to earlier cardiac differentiation in KO mESC cells.

On the other hand, the work with EBs revealed EMT defects that make their cells less motile. This defect in migration seems to raise from increased levels of vinculin. Further expression studies showed a temporal shift in the expression of key genes encoding EMT TFs and prototypical membrane proteins. These differences further confirm that the signalling change in mESC differentiation leads to distinct phenotypical outcomes.

Considering the *in vivo* context, where cardiac development and EMT meet at EndMT, assessing whether there was any change in valve development was the next step. Expression of *Dand5* was confirmed at valve sites in the appropriate

time, and heart valves displayed morphological defects that indicated an inversion of the proper valve leaflet orientation in the absence of DAND5. Valve development is a finely tuned process that begins by patterning of VECs, ending after postnatal remodelling. Interestingly, valve disease is brought by a dysregulation of the same pathways[79], such as Notch, which has been associated with congenital valve defects[144,145] or with valve calcification[146], or BMP, associated with calcification[147], or even TGF-β, involved in valve prolapse[148]. All in all, it is important to fully understand how valves emerge from the HT and how they maintain their function throughout life.

The results on cardiac differentiation enhancement follow previous reports on myocardial hyperplasia of *Dand5* KO mice[97]. Given DAND5's antagonist role of Wnt and TGF-β pathways[89], and their role in cardiac development[33,114], higher signalling activation would be expected following the depletion of common antagonist, with subsequent induction of cardiac differentiation. The results in sections 4.2.2 and 4.2.3 show a decrease in the expression of genes related to these pathways in KO cells. Even though this trend might seem odd, the results on genetic expression show that cardiac fate is induced before the days of differentiation in our dataset, with *Nkx2.5* being expressed on KO cells from day 3 of differentiation[99]. This means that cardiac specification, as well as Wnt and TGF-β activation, precede our dataset. Both canonical Wnt and TGF-β will be later downregulated, as development proceeds and cells need to mature,

evidence that these two pathways are finely tuned during development to induce cardiac differentiation[149–152]. As seen previously at the node, where DAND5 and WNT3 form a regulatory loop[91], perhaps the fine-tuning that ensures proper cardiac development might relay on the extracellular action of DAND5. Upon its depletion, this fine tuning might be disturbed, compromising the proper pattern of activation of Wnt and TGF-β pathways.

The alterations in EMT are not so easy to interpret, as the genetic expression results would predict the opposite of our observations, an exacerbation of the transformation. Such contrast might result from post-translational modifications, or from signalling loops that hinder or accelerate EMT. The expression patterns detailed in 5.2.3 seem to indicate that the depletion of DAND5 removes a brake in genetic expression, allowing for earlier expression of the EMT genes, as well as mesoderm and cardiomyocyte genes[99]. However, the effects of such facilitation are only observable in the induction of mesoderm (*Brachyury* expression[97]) and cardiac features. Section 5.2.1 detailed one of the facts that might be behind lower migratory rates of KO EBs, the way they attach to the substrate. In order to actively migrate, cells must destroy focal contacts, while establishing new ones at the migrating front. As an example, RhoA and YAP promote migration by inducing synthesis of proteins from FA complexes and by controlling the attachment of the cytoskeleton to the membrane[107]. Disassembly and *de novo* assembly of focal points will be limiting factors for migration[126,127,153].

Moreover, focal complexes are also signalling complexes, and they add another layer of regulation for EMT[76,154], with the switch in membrane proteins being one of the hallmarks of the process[61]. The fact that KO EBs have more FAs might result from lower turnover rates, which would explain the lower rates of migration, given the importance of FA turnover for migration[153,155]. The regulation FA turnover is not completely understood, with focal adhesion kinase receptor being one of the most extensively studied[128,129,156]. Despite this, it seems clear that cell migration is highly influenced by the interaction between cell receptors and external cues from the ECM. Given that *Dand5* depletion alters the expression of membrane protein-coding genes, the defects in spreading and migration could result from different membrane proteins patterns in KO cells.

The difference in membrane proteins types and levels, which was detailed in the vinculin immunostaining experiments and the RNAseq dataset, seems to be one of the most significant outcomes of DAND5 depletion, as most DEGs encode proteins that are part of the cell membrane (see CC ORA results on section 4.2.2). As example, integrin β3, one of the DEG of our dataset (*Itgb3*, Figure 4.8) has been found to be associated with influencing EMT and migration within cancer[157]. Moreover, the same integrin subunit has been used as a possible target for heart valve stenosis, since its inhibition prevents smooth muscle cell dysfunction and subsequent pathological valve defects[158]. The relevance of these results lies in the fact that membrane proteins are signalling transductors,

sensors, and ion channels. All these functions make them key players in cell function. The different profiles of membrane protein expression in our dataset might result from different types of cells in KO EBs, but that explanation would lead to starker differences in the pathway ORA results, and not only to the presence of terms related to cardiogenesis. Another possible explanation would be that KO cells establish different kinds of interactions with their microenvironment, evidencing differences in mechanosensing and mechanotransduction. These processes allow cells to manage mechanical forces[72], and will influence cell signalling[132,140]. In zebrafish, for example, the Notch and Wnt pathways have already been reported as being involved in mechanosensing in valvulogenesis[159], which shows the relevance of mechanical forces in cell function.

The *in vivo Dand5* KO model allowed to investigate whether the *in vitro* defects had any translation. Defects in heart valves formation show that the depletion of DAND5 affects their proper organisation. As for the *Dand5* expression location at the valves, it reinforces the notion that valve development results from the interplay of myocardial and endocardial cues[143], namely BMP signalling from the myocardium[80] and endocardial Notch signalling[38].These two pathways have been closely related within valve development[38]. BMP2 has been shown to interact with Notch to pattern VECs to undergo EndMT and form valves[134,160].

Increasing the levels of this BMP, which is upregulated in *Dand5* KO EBs[99], could be the explanation for the morphological defects on Figure 5.7.

The results from this work can contribute to better understand how different signalling pathways regulate each other, as DAND5 is able to target different ligands. The effect its depletion has in genetic expression is remarkable, as is the consequent change in mESC differentiation potential, inducing stronger cardiomyocyte differentiation. Future studies that try to modulate DAND5 could improve cardiomyocyte differentiation protocols. As DAND5 inhibition promotes cardiac progenitors' proliferation, activation of its targets at the right time in stem cell differentiation could be a good strategy to increase the cellular yield. Reversely, understanding the antagonist action of DAND5 and its different targets, might contribute towards devising strategies that are able to activate such targets.

Additional studies are necessary to fully understand DAND5's involvement in development and cell function. Our genetic expression data fails to capture all the possible post-translational modifications that will dictate the effective outcome of gene expression. Membrane proteins, namely integrins and ECM-binding proteins, should be assessed during EB differentiation, as differences in their content and type will have an impact on cells behaviour and state. At the same time, evaluating how KO EBs interact with substrates with different stiffness would help clarifying whether DAND5 is involved in the cells' perception or response to

mechanical cues. Furthermore, rescue experiments would also be informative, even though optimizing them might be difficult, not only in terms of protein levels, but also regarding protein delivery. As DAND5 acts extracellularly and it seems to be expressed only at specific time points, directly supplementing EBs could not be as informative as expected, since the dose delivered would be difficult to optimize, as would delivery strategies, given the spontaneous and generally disorganised differentiation and organisation of EBs. An alternative strategy based on mESCs harbouring an inducible gene expression system could be devised. Even though it would not solve the expression location question, it could help understand how DAND5 modulates its target pathways, which have been reported as having strong dose-dependent outcomes[161–163].

In face of the elusiveness of its role and mechanism, studying the phenotypes resulting from DAND5 depletion, over expression, or conditional expression is still a valuable strategy. Chapter 4 details the impact that DAND5 absence has in EB differentiation, significantly altering genetic expression and signalling pathways. In the same way, further investigating valve development in KO mice would also be useful, since pathological situations seem to share signalling features of embryonic development[79,88]. As BMP2, BMP4, and BMP7 have been strongly associated with valve patterning[81,164], with a significant degree of redundancy, a systematic evaluation of valve defects in *Dand5* KO mice is also warranted, to assess the impact of this antagonist in overall valve development.

Assessing valve structure at more timepoints during development would widen the picture we present here, since postnatal valve morphology and function will be the ultimate read-outs from the disruption caused by *Dand5* depletion. Moreover, explant experiments using mouse valve cushions could provide further information on how EndMT and subsequent valve development are altered in our KO mice.

Understanding the influence of DAND5 in EMT, mechanotransduction, and cell transformation could be useful to further understand its role in development. Furthermore, and bearing in mind the reports associating DAND5 with cancer progression[165–167], studying how this antagonist influences signalling could be useful for new therapeutical avenues in certain types of cancer, besides its already proven value in predicting poor survival in breast cancer[166]. This work could also be translated into cardiovascular diseases, as DAND5 mutations have been implicated in cardiovascular congenital defects[98], and several iPSC cell lines with DAND5 defects have already been generated[168–170]. Combining the use of these cell lines with overall DAND5 knowledge could help improve cardiomyocyte differentiation protocols, required for regenerative medicine approaches, as well as for disease modelling and drug development efforts.

The burden of cardiovascular diseases is very significant, with 19 million deaths being attributed to them in 2020[171]. “Mending broken hearts” remains a challenge, as current therapies have yet to successfully restore cardiac function

mainly due to a poor understanding of heart development and cardiomyocyte maturation. Designing new approaches for these pathologies requires not only investigating new pharmacological targets, but also understanding the cellular events that form and maintain cardiac function. Additionally, the knowledge from *in vitro* studies can help further advance stem cell differentiation and regenerative medicine efforts.

References

1. Wessels, A. & Sedmera, D. Developmental anatomy of the heart: a tale of mice and man. *Physiol. Genomics* **15**, 165–176 (2003).
2. Savolainen, S. M., Foley, J. F. & Elmore, S. A. Histology Atlas of the Developing Mouse Heart with Emphasis on E11.5 to E18.5. *Toxicol. Pathol.* **37**, 395–414 (2009).
3. Morkel, M. *et al.* β-Catenin regulates Cripto- and Wnt3-dependent gene expression programs in mouse axis and mesoderm formation. *Development* **130**, 6283–6294 (2003).
4. Williams, M., Burdsal, C., Periasamy, A., Lewandoski, M. & Sutherland, A. Mouse primitive streak forms in situ by initiation of epithelial to mesenchymal transition without migration of a cell population. *Dev. Dyn.* **241**, 270–283 (2012).
5. Tam, P. P. L., Williams, E. A. & Chan, W. Y. Gastrulation in the mouse embryo: Ultrastructural and molecular aspects of germ layer morphogenesis. *Microsc. Res. Tech.* **26**, 301–328 (1993).
6. Peng, G. *et al.* Molecular architecture of lineage allocation and tissue organization in early mouse embryo. *Nature* **572**, 528–532 (2019).
7. Wilson, V. & Beddington, R. S. P. Cell fate and morphogenetic movement in the late mouse primitive streak. *Mech. Dev.* **55**, 79–89 (1996).

8. Bardot, E. S. & Hadjantonakis, A.-K. Mouse gastrulation: Coordination of tissue patterning, specification and diversification of cell fate. *Mech. Dev.* **163**, 103617 (2020).

9. Saga, Y. *et al.* MesP1 is expressed in the heart precursor cells and required for the formation of a single heart tube. *Development* **126**, 3437–3447 (1999).

10. Meilhac, S. M., Esner, M., Kelly, R. G., Nicolas, J.-F. & Buckingham, M. E. The clonal origin of myocardial cells in different regions of the embryonic mouse heart. *Dev. Cell* **6**, 685–698 (2004).

11. Cai, C.-L. *et al.* Isl1 identifies a cardiac progenitor population that proliferates prior to differentiation and contributes a majority of cells to the heart. *Dev. Cell* **5**, 877–889 (2003).

12. Kelly, R. G., Brown, N. A. & Buckingham, M. E. The arterial pole of the mouse heart forms from Fgf10-expressing cells in pharyngeal mesoderm. *Dev. Cell* **1**, 435–440 (2001).

13. Lescroart, F. *et al.* Early lineage restriction in temporally distinct populations of Mesp1 progenitors during mammalian heart development. *Nat. Cell Biol.* **16**, 829–840 (2014).

14. Bradshaw, L., Chaudhry, B., Hildreth, V., Webb, S. & Henderson, D. J. Dual role for neural crest cells during outflow tract septation in the neural crest-deficient mutant Splotch(2H). *J. Anat.* **214**, 245–257 (2009).

15. del Monte, G. *et al.* Differential Notch signaling in the epicardium is required for cardiac inflow development and coronary vessel morphogenesis. *Circ. Res.* **108**, 824–836 (2011).

16. Cao, J. & Poss, K. D. The epicardium as a hub for heart regeneration. *Nat. Rev. Cardiol.* **15**, 631–647 (2018).

17. Virágh, S., Szabó, E. & Challice, C. E. Formation of the primitive myo- and endocardial tubes in the chicken embryo. *J. Mol. Cell. Cardiol.* **21**, 123–137 (1989).

18. Nakano, A., Nakano, H., Smith, K. A. & Palpant, N. J. The developmental origins and lineage contributions of endocardial endothelium. *Biochim. Biophys. Acta* **1863**, 1937–1947 (2016).

19. Captur, G. *et al.* Morphogenesis of myocardial trabeculae in the mouse embryo. *J. Anat.* **229**, 314–325 (2016).

20. Yang, J. *et al.* Inhibition of Notch2 by Numb/Numblike controls myocardial compaction in the heart. *Cardiovasc. Res.* **96**, 276–285 (2012).

21. Thiery, J. P., Acloque, H., Huang, R. Y. J. & Nieto, M. A. Epithelial-Mesenchymal Transitions in Development and Disease. *Cell* **139**, 871–890 (2009).

22. Brennan, J. *et al.* Nodal signalling in the epiblast patterns the early mouse embryo. *Nature* **411**, 965–969 (2001).

23. Chazaud, C. & Rossant, J. Disruption of early proximodistal patterning and AVE formation in Apc mutants. *Dev. Camb. Engl.* **133**, 3379–3387 (2006).

24. Yamaguchi, T. P., Takada, S., Yoshikawa, Y., Wu, N. & McMahon, A. P. T (Brachyury) is a direct target of Wnt3a during paraxial mesoderm specification. *Genes Dev.* **13**, 3185–3190 (1999).

25. Rivera-Pérez, J. A. & Magnuson, T. Primitive streak formation in mice is preceded by localized activation of Brachyury and Wnt3. *Dev. Biol.* **288**, 363–371 (2005).

26. David, R. *et al.* Induction of MesP1 by Brachyury(T) generates the common multipotent cardiovascular stem cell. *Cardiovasc. Res.* **92**, 115–122 (2011).

27. Chiapparo, G. *et al.* Mesp1 controls the speed, polarity, and directionality of cardiovascular progenitor migration. *J. Cell Biol.* **213**, 463–477 (2016).

28. Waldo, K. L. *et al.* Secondary heart field contributes myocardium and smooth muscle to the arterial pole of the developing heart. *Dev. Biol.* **281**, 78–90 (2005).

29. Bondue, A. *et al.* Mesp1 Acts as a Master Regulator of Multipotent Cardiovascular Progenitor Specification. *Cell Stem Cell* **3**, 69–84 (2008).

30. Vincentz, J. W., Toolan, K. P., Zhang, W. & Firulli, A. B. Hand factor ablation causes defective left ventricular chamber development and compromised adult cardiac function. *PLOS Genet.* **13**, e1006922 (2017).

31. von Both, I. *et al.* Foxh1 is essential for development of the anterior heart field. *Dev. Cell* **7**, 331–345 (2004).

32. Rana, M. S. *et al.* Tbx1 coordinates addition of posterior second heart field progenitor cells to the arterial and venous poles of the heart. *Circ. Res.* **115**, 790–799 (2014).

33. Klaus, A. *et al.* Wnt/β-catenin and Bmp signals control distinct sets of transcription factors in cardiac progenitor cells. *Proc. Natl. Acad. Sci.* **109**, 10921–10926 (2012).

34. Cohen, E. D. *et al.* Wnt/beta-catenin signaling promotes expansion of Isl-1-positive cardiac progenitor cells through regulation of FGF signaling. *J. Clin. Invest.* **117**, 1794–1804 (2007).

35. Ai, D. *et al.* Canonical Wnt signaling functions in second heart field to promote right ventricular growth. *Proc. Natl. Acad. Sci. U. S. A.* **104**, 9319–9324 (2007).

36. Jain, R. *et al.* Integration of Bmp and Wnt signaling by Hopx specifies commitment of cardiomyoblasts. *Science* **348**, aaa6071 (2015).

37. Koefoed, K., Veland, I. R., Pedersen, L. B., Larsen, L. A. & Christensen, S. T. Cilia and coordination of signaling networks during heart development. *Organogenesis* **10**, 108–125 (2014).

38. Garside, V. C., Chang, A. C., Karsan, A. & Hoodless, P. A. Co-ordinating Notch, BMP, and TGF-β signaling during heart valve development. *Cell. Mol. Life Sci.* **70**, 2899–2917 (2013).

39. Grego-Bessa, J. *et al.* Notch signaling is essential for ventricular chamber development. *Dev. Cell* **12**, 415–429 (2007).

40. Zhao, L., Ben-Yair, R., Burns, C. E. & Burns, C. G. Endocardial Notch Signaling Promotes Cardiomyocyte Proliferation in the Regenerating Zebrafish Heart through Wnt Pathway Antagonism. *Cell Rep.* **26**, 546-554.e5 (2019).

41. Bartram, U. *et al.* Double-Outlet Right Ventricle and Overriding Tricuspid Valve Reflect Disturbances of Looping, Myocardialization, Endocardial Cushion Differentiation, and Apoptosis in TGF-β $_2$ –Knockout Mice. *Circulation* **103**, 2745–2752 (2001).

42. Kidokoro, H., Yonei-Tamura, S., Tamura, K., Schoenwolf, G. C. & Saijoh, Y. The heart tube forms and elongates through dynamic cell rearrangement coordinated with foregut extension. *Development* **145**, dev152488 (2018).

43. Chen, Y. *et al.* The Role of Tbx20 in Cardiovascular Development and Function. *Front. Cell Dev. Biol.* **9**, 638542 (2021).

44. Stennard, F. A. *et al.* Cardiac T-box factor Tbx20 directly interacts with Nkx2-5, GATA4, and GATA5 in regulation of gene expression in the developing heart. *Dev. Biol.* **262**, 206–224 (2003).

45. Singh, M. K. *et al.* Tbx20 is essential for cardiac chamber differentiation and repression of Tbx2. *Dev. Camb. Engl.* **132**, 2697–2707 (2005).

46. Shen, T. *et al.* Tbx20 regulates a genetic program essential to adult mouse cardiomyocyte function. *J. Clin. Invest.* **121**, 4640–4654 (2011).

47. Miquerol, L. *et al.* Biphasic Development of the Mammalian Ventricular Conduction System. *Circ. Res.* **107**, 153–161 (2010).

48. van Eif, V. W. W., Stefanovic, S., Mohan, R. A. & Christoffels, V. M. Gradual differentiation and confinement of the cardiac conduction system as indicated by marker gene expression. *Biochim. Biophys. Acta BBA - Mol. Cell Res.* **1867**, 118509 (2020).

49. Mikawa, T. & Hurtado, R. Development of the cardiac conduction system. *Semin. Cell Dev. Biol.* **18**, 90–100 (2007).

50. Hoogaars, W. M. H. *et al.* Tbx3 controls the sinoatrial node gene program and imposes pacemaker function on the atria. *Genes Dev.* **21**, 1098–1112 (2007).

51. Munshi, N. V. Gene Regulatory Networks in Cardiac Conduction System Development. *Circ. Res.* **110**, 1525–1537 (2012).

52. Molecular mechanisms of epithelial–mesenchymal transition | Nature Reviews Molecular Cell Biology. https://www.nature.com/articles/nrm3758.

53. Zhang, A., Aslam, H., Sharma, N., Warmflash, A. & Fakhouri, W. D. Conservation of Epithelial-to-Mesenchymal Transition Process in Neural Crest Cells and Metastatic Cancer. *Cells Tissues Organs* **210**, 151–172 (2021).

54. Ricciardi, M. *et al.* Epithelial-to-mesenchymal transition (EMT) induced by inflammatory priming elicits mesenchymal stromal cell-like immune-modulatory properties in cancer cells. *Br. J. Cancer* **112**, 1067–1075 (2015).

55. Inflammation and EMT: an alliance towards organ fibrosis and cancer progression. *EMBO Mol. Med.* **1**, 303–314 (2009).

56. Lovisa, S. *et al.* Epithelial-to-mesenchymal transition induces cell cycle arrest and parenchymal damage in renal fibrosis. *Nat. Med.* **21**, 998–1009 (2015).

57. Mammoto, T., Jiang, A., Jiang, E. & Mammoto, A. Role of Twist1 Phosphorylation in Angiogenesis and Pulmonary Fibrosis. *Am. J. Respir. Cell Mol. Biol.* **55**, 633–644 (2016).

58. Aktas, B. *et al.* Stem cell and epithelial-mesenchymal transition markers are frequently overexpressed in circulating tumor cells of metastatic breast cancer patients. *Breast Cancer Res. BCR* **11**, R46 (2009).

59. Dongre, A. *et al.* Epithelial-to-mesenchymal Transition contributes to Immunosuppression in Breast Carcinomas. *Cancer Res.* **77**, 3982–3989 (2017).

60. Fischer, K. R. *et al.* Epithelial-to-mesenchymal transition is not required for lung metastasis but contributes to chemoresistance. *Nature* **527**, 472–476 (2015).

61. Yang, J. *et al.* Guidelines and definitions for research on epithelial–mesenchymal transition. *Nat. Rev. Mol. Cell Biol.* **21**, 341–352 (2020).

62. Leerberg, J. M. *et al.* Tension-Sensitive Actin Assembly Supports Contractility at the Epithelial Zonula Adherens. *Curr. Biol.* **24**, 1689–1699 (2014).

63. Mitra, S. K., Hanson, D. A. & Schlaepfer, D. D. Focal adhesion kinase: in command and control of cell motility. *Nat. Rev. Mol. Cell Biol.* **6**, 56–68 (2005).

64. Li, S. & Luo, W. Matrix metalloproteinase 2 contributes to aggressive phenotype, epithelial-mesenchymal transition and poor outcome in nasopharyngeal carcinoma. *OncoTargets Ther.* **12**, 5701–5711 (2019).

65. Simeone, P. *et al.* The multiverse nature of epithelial to mesenchymal transition. *Semin. Cancer Biol.* **58**, 1–10 (2019).

66. Jia, D. *et al.* Testing the gene expression classification of the EMT spectrum. *Phys. Biol.* **16**, 025002 (2019).

67. Chen, Y. & Gridley, T. The SNAI1 and SNAI2 proteins occupy their own and each other's promoter during chondrogenesis. *Biochem. Biophys. Res. Commun.* **435**, 356–360 (2013).

68. Wels, C., Joshi, S., Koefinger, P., Bergler, H. & Schaider, H. Transcriptional activation of ZEB1 by Slug leads to cooperative regulation of the epithelial-mesenchymal transition-like phenotype in melanoma. *J. Invest. Dermatol.* **131**, 1877–1885 (2011).

69. Russell, H. & Pranjol, M. Z. I. Transcription factors controlling E-cadherin down-regulation in ovarian cancer. *Biosci. Horiz. Int. J. Stud. Res.* **11**, hzy010 (2018).

70. Loh, C.-Y. *et al.* The E-Cadherin and N-Cadherin Switch in Epithelial-to-Mesenchymal Transition: Signaling, Therapeutic Implications, and Challenges. *Cells* **8**, 1118 (2019).

71. Lamouille, S., Xu, J. & Derynck, R. Molecular mechanisms of epithelial–mesenchymal transition. *Nat. Rev. Mol. Cell Biol.* **15**, 178–196 (2014).

72. Pattabiraman, S. *et al.* Vimentin protects differentiating stem cells from stress. *Sci. Rep.* **10**, 19525 (2020).

73. Burute, M. *et al.* Polarity Reversal by Centrosome Repositioning Primes Cell Scattering during Epithelial-to-Mesenchymal Transition. *Dev. Cell* **40**, 168–184 (2017).

74. Jung, H.-Y. *et al.* Apical-basal polarity inhibits epithelial-mesenchymal transition and tumour metastasis by PAR-complex-mediated SNAI1 degradation. *Nat. Cell Biol.* **21**, 359–371 (2019).

75. Nelson, W. J. Remodeling epithelial cell organization: transitions between front-rear and apical-basal polarity. *Cold Spring Harb. Perspect. Biol.* **1**, a000513 (2009).

76. Cicchini, C. *et al.* TGFβ-induced EMT requires focal adhesion kinase (FAK) signaling. *Exp. Cell Res.* **314**, 143–152 (2008).

77. Brembeck, F. H., Rosário, M. & Birchmeier, W. Balancing cell adhesion and Wnt signaling, the key role of β-catenin. *Curr. Opin. Genet. Dev.* **16**, 51–59 (2006).

78. Vlad-Fiegen, A., Langerak, A., Eberth, S. & Müller, O. The Wnt pathway destabilizes adherens junctions and promotes cell migration via β-catenin and its target gene cyclin D1. *FEBS Open Bio* **2**, 26–31 (2012).

79. O'Donnell, A. & Yutzey, K. E. Mechanisms of heart valve development and disease. *Development* **147**, dev183020 (2020).

80. Jiao, K. *et al.* An essential role of Bmp4 in the atrioventricular septation of the mouse heart. *Genes Dev.* **17**, 2362–2367 (2003).

81. Liu, W. *et al.* Bmp4 signaling is required for outflow-tract septation and branchial-arch artery remodeling. *Proc. Natl. Acad. Sci.* **101**, 4489–4494 (2004).

82. Rivera-Feliciano, J. & Tabin, C. J. Bmp2 instructs cardiac progenitors to form the heart-valve-inducing field. *Dev. Biol.* **295**, 580–588 (2006).

83. Camenisch, T. D. *et al.* Disruption of hyaluronan synthase-2 abrogates normal cardiac morphogenesis and hyaluronan-mediated transformation of epithelium to mesenchyme. *J. Clin. Invest.* **106**, 349–360 (2000).

84. Kim, K. & Lee, D. ERBB3-dependent AKT and ERK pathways are essential for atrioventricular cushion development in mouse embryos. *PLOS ONE* **16**, e0259426 (2021).

85. Hulin, A. *et al.* Maturation of heart valve cell populations during postnatal remodeling. *Dev. Camb. Engl.* **146**, dev173047 (2019).

86. Peacock, J. D., Lu, Y., Koch, M., Kadler, K. E. & Lincoln, J. Temporal and spatial expression of collagens during murine atrioventricular heart valve development and maintenance. *Dev. Dyn. Off. Publ. Am. Assoc. Anat.* **237**, 3051–3058 (2008).

87. Latif, N., Sarathchandra, P., Taylor, P. M., Antoniw, J. & Yacoub, M. H. Localization and pattern of expression of extracellular matrix components in human heart valves. *J. Heart Valve Dis.* **14**, 218–227 (2005).

88. Freeman, R. V. & Otto, C. M. Spectrum of Calcific Aortic Valve Disease. *Circulation* **111**, 3316–3326 (2005).

89. Marques, S. *et al.* The activity of the Nodal antagonist *Cerl-2* in the mouse node is required for correct L/R body axis. *Genes Dev.* **18**, 2342–2347 (2004).

90. Nolan, K. & Thompson, T. B. The DAN family: Modulators of TGF-β signaling and beyond: The DAN Family. *Protein Sci.* **23**, 999–1012 (2014).

91. Nakamura, T. *et al.* Fluid flow and interlinked feedback loops establish left–right asymmetric decay of Cerl2 mRNA. *Nat. Commun.* **3**, 1322 (2012).

92. Minegishi, K. *et al.* Fluid flow-induced left-right asymmetric decay of Dand5 mRNA in the mouse embryo requires a Bicc1-Ccr4 RNA degradation complex. *Nat. Commun.* **12**, 4071 (2021).

93. Inácio, J. M. *et al.* The Dynamic Right-to-Left Translocation of Cerl2 Is Involved in the Regulation and Termination of Nodal Activity in the Mouse Node. *PLoS ONE* **8**, e60406 (2013).

94. Logan, M., Pagán-Westphal, S. M., Smith, D. M., Paganessi, L. & Tabin, C. J. The Transcription Factor Pitx2 Mediates Situs-Specific Morphogenesis in Response to Left-Right Asymmetric Signals. *Cell* **94**, 307–317 (1998).

95. Larkins, C. E., Bushey Long, A. & Caspary, T. Defective Nodal and Cerl2 expression in the Arl13bhnn mutant node underlie its heterotaxia. *Dev. Biol.* **367**, 15–24 (2012).

96. Saijoh, Y., Oki, S., Ohishi, S. & Hamada, H. Left–right patterning of the mouse lateral plate requires nodal produced in the node. *Dev. Biol.* **256**, 161–173 (2003).

97. Araújo, A. C., Marques, S. & Belo, J. A. Targeted Inactivation of Cerberus Like-2 Leads to Left Ventricular Cardiac Hyperplasia and Systolic Dysfunction in the Mouse. *PLoS ONE* **9**, e102716 (2014).

98. Cristo, F. *et al.* Functional study of DAND5 variant in patients with Congenital Heart Disease and laterality defects. *BMC Med. Genet.* **18**, 77 (2017).

99. Inácio, J. M. *et al.* DAND5 Inactivation Enhances Cardiac Differentiation in Mouse Embryonic Stem Cells. *Front. Cell Dev. Biol.* **9**, 629430 (2021).

100. Dobin, A. & Gingeras, T. R. Mapping RNA-seq Reads with STAR. *Curr. Protoc. Bioinforma.* **51**, 11.14.1-11.14.19 (2015).

101. Liao, Y., Smyth, G. K. & Shi, W. The R package Rsubread is easier, faster, cheaper and better for alignment and quantification of RNA sequencing reads. *Nucleic Acids Res.* **47**, e47 (2019).

102. McCarthy, D. J., Chen, Y. & Smyth, G. K. Differential expression analysis of multifactor RNA-Seq experiments with respect to biological variation. *Nucleic Acids Res.* **40**, 4288–4297 (2012).

103. Ritchie, M. E. *et al.* limma powers differential expression analyses for RNA-sequencing and microarray studies. *Nucleic Acids Res.* **43**, e47 (2015).

104. Liao, Y., Wang, J., Jaehnig, E. J., Shi, Z. & Zhang, B. WebGestalt 2019: gene set analysis toolkit with revamped UIs and APIs. *Nucleic Acids Res.* **47**, W199–W205 (2019).

105. Livak, K. J. & Schmittgen, T. D. Analysis of relative gene expression data using real-time quantitative PCR and the 2(-Delta Delta C(T)) Method. *Methods San Diego Calif* **25**, 402–408 (2001).

106. Schindelin, J. *et al.* Fiji: an open-source platform for biological-image analysis. *Nat. Methods* **9**, 676–682 (2012).

107. Nardone, G. *et al.* YAP regulates cell mechanics by controlling focal adhesion assembly. *Nat. Commun.* **8**, 15321 (2017).

108. Koike, M., Sakaki, S., Amano, Y. & Kurosawa, H. Characterization of embryoid bodies of mouse embryonic stem cells formed under various culture conditions and estimation of differentiation status of such bodies. *J. Biosci. Bioeng.* **104**, 294–299 (2007).

109. ten Berge, D. *et al.* Wnt signaling mediates self-organization and axis formation in embryoid bodies. *Cell Stem Cell* **3**, 508–518 (2008).

110. Wilson, J. L. *et al.* Single-cell analysis of embryoid body heterogeneity using microfluidic trapping array. *Biomed. Microdevices* **16**, 79–90 (2014).

111. Camacho-Aguilar, E. & Warmflash, A. Chapter Nine - Insights into mammalian morphogen dynamics from embryonic stem cell systems. in *Current Topics in Developmental Biology* (eds. Small, S. & Briscoe, J.) vol. 137 279–305 (Academic Press, 2020).

112. Morgani, S. M. & Hadjantonakis, A.-K. Chapter Thirteen - Signaling regulation during gastrulation: Insights from mouse embryos and in vitro systems. in *Current Topics in Developmental Biology* (eds. Small, S. & Briscoe, J.) vol. 137 391–431 (Academic Press, 2020).

113. Chan, S. S.-K. *et al.* Mesp1 Patterns Mesoderm into Cardiac, Hematopoietic, or Skeletal Myogenic Progenitors in a Context-Dependent Manner. *Cell Stem Cell* **12**, 587–601 (2013).

114. Ruiz-Villalba, A., Hoppler, S. & van den Hoff, M. J. B. Wnt signaling in the heart fields: Variations on a common theme: Wnt Signaling in the Heart Fields. *Dev. Dyn.* **245**, 294–306 (2016).

115. Mp, P., Ln, P. & Ssk, C. Dual TGFβ and Wnt inhibition promotes Mesp1-mediated mouse pluripotent stem cell differentiation into functional cardiomyocytes. *Dev. Growth Differ.* **62**, (2020).

116. Rogers, K. W. *et al.* Nodal patterning without Lefty inhibitory feedback is functional but fragile. *eLife* **6**, e28785.

117. Kim, D.-K., Cha, Y., Ahn, H.-J., Kim, G. & Park, K.-S. *Lefty1* and *Lefty2* Control the Balance Between Self-Renewal and Pluripotent Differentiation of Mouse Embryonic Stem Cells. *Stem Cells Dev.* **23**, 457–466 (2014).

118. Bandyopadhyay, A. *et al.* Genetic Analysis of the Roles of BMP2, BMP4, and BMP7 in Limb Patterning and Skeletogenesis. *PLOS Genet.* **2**, e216 (2006).

119. Yang, Y.-P., Anderson, R. M. & Klingensmith, J. BMP antagonism protects Nodal signaling in the gastrula to promote the tissue interactions underlying mammalian forebrain and craniofacial patterning. *Hum. Mol. Genet.* **19**, 3030–3042 (2010).

120. Souilhol, C. *et al.* NOTCH activation interferes with cell fate specification in the gastrulating mouse embryo. *Development* **142**, 3649–3660 (2015).

121. Chen, J., Imanaka, N., Chen, J. & Griffin, J. D. Hypoxia potentiates Notch signaling in breast cancer leading to decreased E-cadherin expression and increased cell migration and invasion. *Br. J. Cancer* **102**, 351–360 (2010).

122. Ji, Z. *et al.* Hypoxia-inducible factor-2α promotes EMT in esophageal squamous cell carcinoma through the Notch pathway. *Adv. Clin. Exp. Med. Off. Organ Wroclaw Med. Univ.* **31**, 795–805 (2022).

123. Timmerman, L. A. *et al.* Notch promotes epithelial-mesenchymal transition during cardiac development and oncogenic transformation. *Genes Dev.* **18**, 99–115 (2004).

124. Howard, S., Deroo, T., Fujita, Y. & Itasaki, N. A Positive Role of Cadherin in Wnt/β-Catenin Signalling during Epithelial-Mesenchymal Transition. *PLoS ONE* **6**, e23899 (2011).

125. Shao, S. *et al.* Notch1 signaling regulates the epithelial–mesenchymal transition and invasion of breast cancer in a Slug-dependent manner. *Mol. Cancer* **14**, 28 (2015).

126. Besson, A., Davy, A., Robbins, S. M. & Yong, V. W. Differential activation of ERKs to focal adhesions by PKC epsilon is required for PMA-induced adhesion and migration of human glioma cells. *Oncogene* **20**, 7398–7407 (2001).

127. Yu, H. *et al.* Inhibition of cell migration by focal adhesion kinase: Time-dependent difference in integrin-induced signaling between endothelial and hepatoblastoma cells. *Int. J. Mol. Med.* **41**, 2573–2588 (2018).

128. Hu, Y.-L. *et al.* FAK and paxillin dynamics at focal adhesions in the protrusions of migrating cells. *Sci. Rep.* **4**, 6024 (2014).

129. Bjerke, M. A., Dzamba, B. J., Wang, C. & DeSimone, D. W. FAK is required for tension-dependent organization of collective cell movements in Xenopus mesendoderm. *Dev. Biol.* **394**, 340–356 (2014).

130. Chen, J.-C. *et al.* BMP-7 Enhances Cell Migration and αvβ3 Integrin Expression via a c-Src-Dependent Pathway in Human Chondrosarcoma Cells. *PLOS ONE* **9**, e112636 (2014).

131. Li, L., Okura, M. & Imamoto, A. Focal Adhesions Require Catalytic Activity of Src Family Kinases To Mediate Integrin-Matrix Adhesion. *Mol. Cell. Biol.* **22**, 1203–1217 (2002).

132. Sales, A. *et al.* Differential bioactivity of four BMP-family members as function of biomaterial stiffness. *Biomaterials* **281**, 121363 (2022).

133. Richter, A. *et al.* BMP4 Promotes EMT and Mesodermal Commitment in Human Embryonic Stem Cells via SLUG and MSX2. *STEM CELLS* **32**, 636–648 (2014).

134. Papoutsi, T., Luna-Zurita, L., Prados, B., Zaffran, S. & de la Pompa, J. L. Bmp2 and Notch cooperate to pattern the embryonic endocardium. *Dev. Camb. Engl.* **145**, dev163378 (2018).

135. Luna-Zurita, L. *et al.* Integration of a Notch-dependent mesenchymal gene program and Bmp2-driven cell invasiveness regulates murine cardiac valve formation. *J. Clin. Invest.* **120**, 3493–3507 (2010).

136. Erusappan, P., Alam, J., Lu, N., Zeltz, C. & Gullberg, D. Integrin α11 cytoplasmic tail is required for FAK activation to initiate 3D cell invasion and ERK-mediated cell proliferation. *Sci. Rep.* **9**, 15283 (2019).

137. Schiller, H. B. *et al.* β1- and αv-class integrins cooperate to regulate myosin II during rigidity sensing of fibronectin-based microenvironments. *Nat. Cell Biol.* **15**, 625–636 (2013).

138. Liebner, S. *et al.* Beta-catenin is required for endothelial-mesenchymal transformation during heart cushion development in the mouse. *J. Cell Biol.* **166**, 359–367 (2004).

139. Przybyla, L., Muncie, J. M. & Weaver, V. M. Mechanical Control of Epithelial-to-Mesenchymal Transitions in Development and Cancer. *Annu. Rev. Cell Dev. Biol.* **32**, 527–554 (2016).

140. Lü, D., Luo, C., Zhang, C., Li, Z. & Long, M. Differential regulation of morphology and stemness of mouse embryonic stem cells by substrate stiffness and topography. *Biomaterials* **35**, 3945–3955 (2014).

141. Wei, Q. *et al.* BMP-2 Signaling and Mechanotransduction Synergize to Drive Osteogenic Differentiation via YAP/TAZ. *Adv. Sci.* **7**, 1902931 (2020).

142. Qu, X., Harmelink, C. & Baldwin, H. S. Endocardial-Myocardial Interactions During Early Cardiac Differentiation and Trabeculation. *Front. Cardiovasc. Med.* **9**, 857581 (2022).

143. Wang, Y. *et al.* Endocardial to Myocardial Notch-Wnt-Bmp Axis Regulates Early Heart Valve Development. *PLoS ONE* **8**, e60244 (2013).

144. Bosse, K. *et al.* Endothelial nitric oxide signaling regulates Notch1 in aortic valve disease. *J. Mol. Cell. Cardiol.* **60**, 27–35 (2013).

145. Godby, R. C. *et al.* Cross Talk between NOTCH Signaling and Biomechanics in Human Aortic Valve Disease Pathogenesis. *J. Cardiovasc. Dev. Dis.* **1**, 237–256 (2014).

146. White, M. P. *et al.* NOTCH1 regulates matrix gla protein and calcification gene networks in human valve endothelium. *J. Mol. Cell. Cardiol.* **84**, 13–23 (2015).

147. Gomez-Stallons, M. V., Wirrig-Schwendeman, E. E., Hassel, K. R., Conway, S. J. & Yutzey, K. E. Bone Morphogenetic Protein Signaling Is Required for Aortic Valve Calcification. *Arterioscler. Thromb. Vasc. Biol.* **36**, 1398–1405 (2016).

148. Tang, Q., McNair, A. J., Phadwal, K., Macrae, V. E. & Corcoran, B. M. The Role of Transforming Growth Factor-β Signaling in Myxomatous Mitral Valve Degeneration. *Front. Cardiovasc. Med.* **9**, 872288 (2022).

149. Gessert, S. & Kühl, M. The Multiple Phases and Faces of Wnt Signaling During Cardiac Differentiation and Development. *Circ. Res.* **107**, 186–199 (2010).

150. Naito, A. T. *et al.* Developmental stage-specific biphasic roles of Wnt/β-catenin signaling in cardiomyogenesis and hematopoiesis. *Proc. Natl. Acad. Sci.* **103**, 19812–19817 (2006).

151. Laflamme, M. A. *et al.* Cardiomyocytes derived from human embryonic stem cells in pro-survival factors enhance function of infarcted rat hearts. *Nat. Biotechnol.* **25**, 1015–1024 (2007).

152. Watabe, T. & Miyazono, K. Roles of TGF-β family signaling in stem cell renewal and differentiation. *Cell Res.* **19**, 103–115 (2009).

153. Nagano, M., Hoshino, D., Koshikawa, N., Akizawa, T. & Seiki, M. Turnover of Focal Adhesions and Cancer Cell Migration. *Int. J. Cell Biol.* **2012**, 1–10 (2012).

154. Lehembre, F. *et al.* NCAM-induced focal adhesion assembly: a functional switch upon loss of E-cadherin. *EMBO J.* **27**, 2603–2615 (2008).

155. Owen, K. A. *et al.* Regulation of lamellipodial persistence, adhesion turnover, and motility in macrophages by focal adhesion kinase. *J. Cell Biol.* **179**, 1275–1287 (2007).

156. Sieg, D. J. *et al.* FAK integrates growth-factor and integrin signals to promote cell migration. *Nat. Cell Biol.* **2**, 249–256 (2000).

157. Kariya, Y., Oyama, M., Suzuki, T. & Kariya, Y. αvβ3 Integrin induces partial EMT independent of TGF-β signaling. *Commun. Biol.* **4**, 490 (2021).

158. Misra, A. *et al.* Integrin β3 inhibition is a therapeutic strategy for supravalvular aortic stenosis. *J. Exp. Med.* **213**, 451–463 (2016).

159. Paolini, A., Fontana, F., Pham, V.-C., Rödel, C. J. & Abdelilah-Seyfried, S. Mechanosensitive Notch-Dll4 and Klf2-Wnt9 signaling pathways intersect in guiding valvulogenesis in zebrafish. *Cell Rep.* **37**, 109782 (2021).

160. Prados, B. *et al.* Myocardial Bmp2 gain causes ectopic EMT and promotes cardiomyocyte proliferation and immaturity. *Cell Death Dis.* **9**, 1–15 (2018).

161. Lu, T., Tian, L., Han, Y., Vogelbaum, M. & Stark, G. R. Dose-dependent cross-talk between the transforming growth factor-beta and interleukin-1 signaling pathways. *Proc. Natl. Acad. Sci. U. S. A.* **104**, 4365–4370 (2007).

162. Robertson, E. J. Dose-dependent Nodal/Smad signals pattern the early mouse embryo. *Semin. Cell Dev. Biol.* **32**, 73–79 (2014).

163. Fragiadaki, M. *et al.* High doses of TGF-β potently suppress type I collagen via the transcription factor CUX1. *Mol. Biol. Cell* **22**, 1836–1844 (2011).

164. Goldman, D. C., Donley, N. & Christian, J. L. Genetic interaction between Bmp2 and Bmp4 reveals shared functions during multiple aspects of mouse organogenesis. *Mech. Dev.* **126**, 117–127 (2009).

165. Miao, X. *et al.* Elevated serum DAND5 is associated with metastasis and predicts poor prognosis in colorectal cancer. *United Eur. Gastroenterol. J.* **5**, 725–734 (2017).

166. Chi, Y. *et al.* The BMP inhibitor DAND5 in serum predicts poor survival in breast cancer. *Oncotarget* **7**, 14951–14962 (2016).

167. Elevated serum DAND5 is associated with metastasis and predicts poor prognosis in colorectal cancer - Xiaofei Miao, Ye Zhang, Jialin Sun, Songkui Cui, Qingyang Meng, Kuiyu Zhu, Xingqian Hu, Tong Wang, 2017. https://journals.sagepub.com/doi/full/10.1177/2050640616674838.

168. Cristo, F. *et al.* Generation of human iPSC line from a patient with laterality defects and associated congenital heart anomalies carrying a DAND5 missense alteration. *Stem Cell Res.* **25**, 152–156 (2017).

169. Inácio, J. M., Almeida, M., Cristo, F. & Belo, J. A. Generation of a gene-corrected human induced pluripotent stem cell line derived from a patient with laterality defects and congenital heart anomalies with a c.455G > A alteration in DAND5. *Stem Cell Res.* **42**, 101677 (2020).

170. Pars, S. *et al.* Generation and characterization of a human iPS cell line from a patient-related control to study disease mechanisms associated with DAND5 p.R152H alteration. *Stem Cell Res.* **29**, 202–206 (2018).

171. Tsao, C. W. *et al.* Heart Disease and Stroke Statistics—2022 Update: A Report From the American Heart Association. *Circulation* **145**, (2022).